Chemosphere, Volume 337, October 2023, Article number 139404
DOI:10.1016/j.chemosphere.2023.139404

Harnessing the power of natural minerals: a comprehensive review of their application as heterogeneous catalysts in advanced oxidation processes for organic pollutant degradation

Hongwen Liu[1], Xingyang Li[1], Xiuxiu Zhang[1], Frederic Coulon[2], Chongqing Wang[1]*

[1] School of Chemical Engineering, Zhengzhou University, Zhengzhou 450001, China;

[2] School of Water, Energy and Environment, Cranfield University, Cranfield, MK43 0AL, United Kingdom; Email: f.coulon@cranfield.ac.uk.

*Corresponding author: Chongqing Wang, E-mail: zilangwang@126.com, ORCID: 0000-0003-2580-9263.

Abstract: The release of untreated wastewater into water bodies has become a significant environmental concern, resulting in the accumulation of refractory organic pollutants that pose risks to human health and ecosystems. Wastewater treatment methods, including biological, physical, and chemical techniques, have limitations in achieving complete removal of the refractory pollutants. Chemical methods, particularly advanced oxidation processes (AOPs), have gained special attention for their strong oxidation capacity and minimal secondary pollution. Among the various catalysts used in AOPs, natural minerals offer distinct advantages, such as low cost, abundant resources, and environmental friendliness. Currently, the utilization of natural minerals as catalysts in AOPs lacks thorough investigation and review. This work addresses the need for a comprehensive review of natural minerals as catalysts in AOPs. The structural characteristics and catalytic performance of different natural minerals are discussed, emphasizing their specific roles in AOPs. Furthermore, the review analyzes the influence of process factors, including catalyst dosage, oxidant addition, pH value, and temperature, on the catalytic performance of natural minerals. Strategies for enhancing the catalytic efficiency of AOPs mediated by natural minerals are explored, mainly including physical fields, reductant addition, and cocatalyst utilization. The review also examines the practical application prospects and main challenges associated with the use of natural minerals as heterogeneous catalysts in AOPs. This work contributes to the development of sustainable and efficient approaches for organic pollutant degradation in wastewater.

Keywords: Natural minerals, Wastewater treatment, Advanced oxidation processes, Organic pollutants.

Published by Elsevier. This is the Author Accepted Manuscript issued with: Creative Commons Attribution Non-Commercial No Derivatives License (CC:BY:NC:ND 4.0).
The final published version (version of record) is available online at DOI:10.1016/j.chemosphere.2023.139404. Please refer to any applicable publisher terms of use.

Table of Contents

1. Introduction

2. Advanced oxidation processes based on HPO or PSs

3. Natural minerals

    3.1 Iron sulfide minerals

    3.2 Iron oxide minerals

    3.3 Bimetallic minerals

    3.4 Multi-metal minerals

4. Natural minerals for heterogeneous AOPs

    4.1 Iron sulfide minerals as catalysts

    4.2 Iron oxide minerals as catalysts

    4.3 Bimetallic minerals as catalysts

    4.4 Multi-metal minerals as catalysts

5. The influence of process factors

    5.1 Effects of catalyst dosage and particle size

    5.2 Effects of oxidant dosage

    5.3 Effects of pH

    5.4 Effects of inorganic anions

    5.5 Effects of reaction temperature

6. Strategies for improving catalytic activity

    6.1 External physical fields

    6.2 Adding reductants

    6.3 Minerals as cocatalyst

7. Research perspectives

8. Conclusions

References

1. Introduction

In recent years, the pollution of water resources by various pollutants has emerged as a significant threat to human health and the environment (Andrews and Hennet, 2022; Lancia et al., 2022). The continuous discharge of wastewater, resulting from human activities and industrial processes, has led to the accumulation of refractory organic pollutants in water bodies (Dutt et al., 2020; Liu et al., 2022c). These refractory organic pollutants pose significant challenges for complete removal through conventional treatment methods. While biological, physical, and chemical methods are employed in wastewater treatment (Wang et al., 2022a), advanced oxidation processes (AOPs) stand out for their efficiency in decomposing refractory organic pollutants (Zhang et al., 2022d). AOPs have gained considerable attention due to their strong oxidation capabilities and minimal secondary pollution (Wang et al., 2022h; Yao et al., 2022). AOPs involve the activation of oxidants such as hydrogen peroxide (HPO) or persulfates (PSs) to generate reactive oxygen species (ROS), such as hydroxyl radicals (·OH), sulfate radicals ($SO_4^{\cdot-}$), superoxide radicals ($O_2^{\cdot-}$), capable of decomposing and even mineralizing organic pollutants into non-toxic substances.

The choice of catalyst in AOPs has always been the focus of researchers. Loffredo et al. loaded iron and manganese on ZrO_2 to prepare a bimetallic catalyst, in which the bimetallic active sites of Fe and Mn could achieve the maximum activation of peroxymonosulfate, and the mineralization rates of different pollutants were above 90.0% (Loffredo et al., 2023). In Lu's study, Co-doped on ZnAl-layered double hydroxides was prepared by one-step hydrothermal method and used as a peroxymonosulfate activator, and the degradation of pollutants could reach 91.5% within 15 min (Lu et al., 2023). While synthetic catalysts, including carbon-based catalysts and transition metal-containing materials, exhibit excellent performance, they suffer from drawbacks such as high cost, complex process, and potential secondary pollution (Sun et al., 2021c; Wang et al., 2022e; Wang et al., 2023c). In contrast, natural minerals offer several advantages as catalysts, including their low cost, abundance, and environmental friendliness. Natural minerals possess unique structures and properties that enable them to remain stable in chemical solutions. For example, iron-based minerals can gradually release iron ions, spontaneously adjusting solution pH and promoting catalysis (Zeng et al., 2023). Moreover, natural minerals possess complex compositions, and certain trace elements can synergistically enhance catalytic activity.

Despite the significant catalytic effects of natural minerals in AOPs, there is a lack of comprehensive

reviews in this field, limiting our understanding and guidance for further research. This comprehensive review addresses the need for a thorough summary of natural minerals as heterogeneous catalysts in AOPs (Fig. 1). The work involves the structural characteristics and catalytic performance of different natural minerals, emphasizing their specific roles in AOPs. The influence of process factors on the catalytic capacity of natural minerals is discussed, shedding light on critical factors influencing their performance. Strategies to enhance the catalytic efficiency of AOPs using natural minerals are summarized, along with an analysis of the current challenges and application prospects. By offering insights into the potential of natural minerals as heterogeneous catalysts in AOPs, this review contributes to the development of efficient and sustainable strategies for organic pollutant degradation in wastewater treatment.

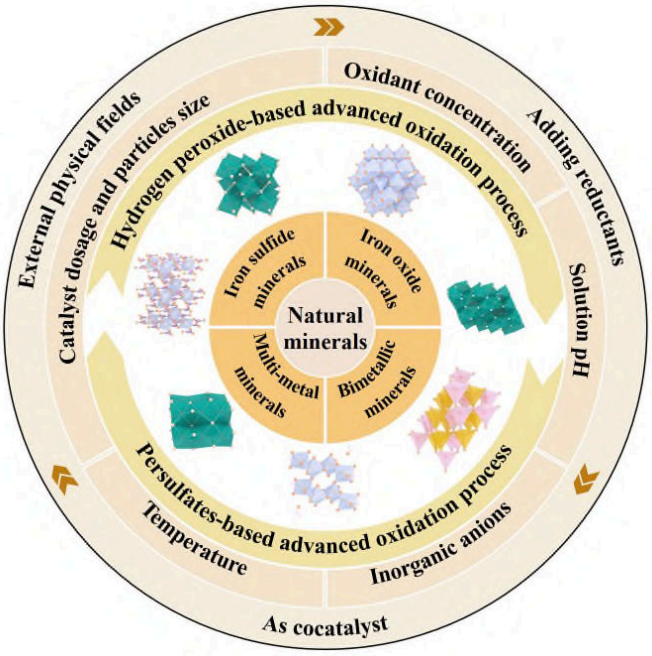


Fig. 1. The summary of natural minerals as heterogeneous catalysts in AOPs.

2. Advanced oxidation processes based on HPO or PSs

AOPs represent a class of water treatment methods that rely on highly reactive free radicals with strong oxidizability. These processes aim to achieve the complete mineralization of organic pollutants, resulting in the production of non-toxic substances (Wang et al., 2021b). Free radicals are defined as atoms or groups of atoms that possess unpaired electrons and are primarily formed by the cleavage of the O-O bond in HPO or PSs. Various methods can be employed to generate free radicals, including high

temperature, microwave radiation, electricity, light, and catalysts. Depending on the specific approach used, AOPs can be categorized into Fenton process, electrochemical oxidation, photocatalytic oxidation, microwave-assisted oxidation, and the combinations of them (Fan et al., 2021; Liu et al., 2023a; Wang et al., 2023b).

AOPs based on HPO can be classified into homogeneous Fenton and heterogeneous Fenton processes. The Fenton reaction was discovered in 1894 when tartaric acid was rapidly decomposed by the addition of Fe^{2+} and H_2O_2 to an acidic solution (Qi et al., 2023; Jiang et al., 2022b). This mixture, known as Fenton reagent, exhibits high oxidizing capabilities. The combination of Fe^{2+} and H_2O_2 generates active radicals such as ·OH and ·OOH through Eq. 1-2, initiating a chain of subsequent reactions (Han et al., 2023; Dolatabadi et al., 2021). The conventional Fenton process has certain limitations, including the instability of H_2O_2, a narrow pH range for effective application, and the propensity to produce sludge during the catalytic process (Pan et al., 2023). To address these issues in industrial applications, researchers have explored the use of iron-based catalysts as replacement of soluble Fe^{2+}, resulting in heterogeneous AOPs (Xu et al., 2023). Fig. a depicts the reaction mechanism of both homogeneous and heterogeneous Fenton reactions. In heterogeneous Fenton systems, some iron ions are released into the solution from the solid catalysts, allowing for the coexistence of both homogeneous and heterogeneous reactions. In Huang's study, the homogeneous reaction predominantly contributed to the removal of orange II from natural chalcopyrite, while the heterogeneous reaction accounted for approximately 20.0% of pollutants removal and significantly enhanced the degradation of orange II (Huang et al., 2020).

$$Fe^{2+} + H_2O_2 \rightarrow Fe^{3+} + \cdot OH + OH^- \quad (1)$$

$$Fe^{3+} + H_2O_2 \rightarrow Fe^{2+} + HOO \cdot + H^+ \quad (2)$$

Compared to the ·OH with an oxidation potential of 1.9-2.7 V, the $SO_4^{\cdot-}$ generated through the activation of PSs exhibits higher oxidation capacity (2.5-3.1 V) and longer lifespan (Wang and Wang, 2018a; Wang et al., 2022f; Dolatabadi et al., 2023). Additionally, PSs possesses relatively stable properties and can be easily stored and transported in its solid form at room temperature. PSs is categorized into peroxymonosulfate (PMS, HSO_5^-) and peroxydisulfate (PDS, $S_2O_8^{2-}$) based on the amount of sulfur in its molecule (Wang et al., 2021a). As illustrated in Fig. b, PDS can be activated through different methods, including the addition of energy (thermal, UV, ultrasonic, microwave, etc.),

chemicals, or transition metals. Studies have demonstrated that PSs activation can effectively eliminate refractory organic pollutants via both free radical and non-free radical pathways (Fig. c). These pollutants include polycyclic aromatic hydrocarbons, perfluorinated compounds, volatile organic compounds, and others (Mora and Rosso, 2022; Yang et al., 2020).

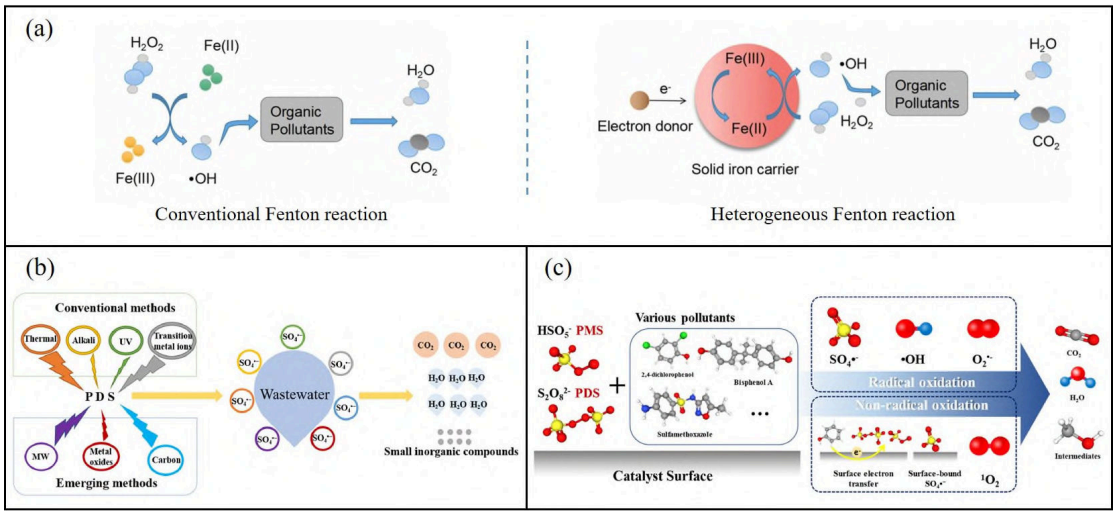


Fig. 2. (a) The reaction mechanism of homogeneous and heterogeneous Fenton reactions. Reprinted with permission of Elsevier from Chen et al., 2023a. (b) The activation method of PDS. Reprinted with permission of Elsevier from Tian et al., 2022. (c) The pathway of organic pollutants removal in PS-AOPs. Reprinted with permission of Elsevier from Guo et al., 2022b.

3. Natural minerals

Natural minerals can be broadly categorized into clay minerals and metallic minerals. Clay minerals consist of water-containing silicates or silico-aluminates, with their chemical composition primarily composed of SiO_2, and Al_2O_3. Additionally, they may contain varying amounts of Fe_2O_3, MgO, and small quantities of K_2O, Na_2O, CaO_2, and other elements (Novikau and Lujaniene, 2022). Due to the low content of active metals in clay minerals, they cannot be used directly as catalysts. In contrast, metallic minerals possess high content of active metals (Elmacı et al., 2015; Elmacı, 2020; Elmacı et al., 2020), and thus can be used as efficient activators of HPO and PSs without the need for complex synthesis processes.

3.1 Iron sulfide minerals

Fig. shows the crystal structures of different iron-based minerals. Pyrite, a widely distributed iron sulfide mineral, is formed under various geological conditions, and primarily composed of FeS_2. The

composition of pure pyrite consists of 46.5% Fe and 53.5% S. However, natural pyrite may contain trace elements such as Cu, Ni, Co, Sb, and As, resulting in slight variations in the Fe and S content. The specific surface area of natural pyrite is relatively small, which limits its adsorption capacity for pollutants removal. The crystal structure of pyrite closely resembles that of NaCl. Iron atoms are arranged in a face-centered cubic pattern, occupying the positions of Na in the unit cell face center and peak. Sulfur atoms form S_2^{2-} units with a dumbbell shape, replacing Cl and positioned in the center of the edge and body of the unit cell (Zhang et al., 2022b). Additionally, each sulfur atom is connected to three iron atoms, forming a tetrahedron, while each iron atom is surrounded by six sulfur atoms to create an octahedron. The octahedron slightly distorts due to inter-atomic coordination effects.

Pyrrhotite is a dark yellow mineral commonly found in copper-nickel sulfide deposits. It is prone to weathering into limonite when exposed to the atmosphere. The chemical formula of pyrrhotite is $Fe_{1-x}S$ (x = 0-0.17), where a portion of Fe^{2+} is replaced by Fe^{3+} ions. To maintain charge conservation, partial vacancies occur in the original positions of Fe^{2+}, resulting in a relatively higher sulfur content and classifying pyrrhotite as non-stoichiometric. The presence of iron vacancies not only affects the chemical composition but also influences the crystal structure. Pyrrhotite commonly exhibits monoclinic and hexagonal systems, with the specific structure primarily determined by its composition. As the relative sulfur content increases, the crystal structure transitions from a hexagonal system to a monoclinic system. Natural pyrrhotite possesses soft magnetic properties, with a saturation magnetization of 6 $emu \cdot g^{-1}$, coercivity of 16 Oe, and remanence of 0.056 $emu \cdot g^{-1}$, enabling magnetic recovery of natural pyrrhotite in solution (Xia et al., 2017a).

In addition to pyrite and pyrrhotite, mackinawite (FeS) is another iron sulfide mineral. Initially discovered in America, mackinawite is the primary corrosion product formed when iron reacts with hydrogen sulfide at low temperatures. It is commonly found in association with pyrite or chalcopyrite. Mackinawite exhibits a tetragonal crystal system, with iron atoms located at the center of S tetrahedra (Wen et al., 2017). These FeS_4 tetrahedra are stacked along specific crystal axes, forming contiguous layers of tetrahedral tablets. Natural mackinawite is a metastable mineral that readily transforms into pyrite or pyrrhotite under high temperatures or specific conditions.

3.2 Iron oxide minerals

Currently, sixteen types of iron oxide minerals are known, with magnetite, hematite, and goethite

being the most common (Lai et al., 2021; Zeng et al., 2023). These minerals are widely present in soil and sedimentary rock. The crystal structures of iron oxide minerals can undergo mutual transformations under specific conditions (Ponomar, 2018). Hematite (α-Fe_2O_3) and maghemite (γ-Fe_2O_3) have the same chemical composition but different crystal structures (Ashraf et al., 2022). Hematite possesses a corundum-type structure with excellent thermal stability, whereas magnetite has relatively lower thermal stability. Magnetite and maghemite share similar crystal structures, with magnetite adopting an inverse spinel structure, and maghemite exhibiting a defective spinel structure. Both minerals exhibit strong magnetism (Frison et al., 2013). Compared to hematite, magnetite and maghemite are more easily separated and recycled. Maghemite contains numerous vacancies that facilitate the adsorption of oxidizing agents and pollutants (Shokrollahi, 2017; Tuutijärvi et al., 2009). However, some studies have indicated that untreated maghemite exhibits unsatisfactory catalytic activity. Most research focuses on modifying maghemite by adding carbon materials or doping transition metals and oxides to enhance its catalytic activity (Liu et al., 2022b). The use of natural maghemite alone in the HPO or PSs system is rare.

The group of iron oxyhydroxides includes goethite, ferrihydrite, and lepidocrocite (Molamahmood et al., 2022). The chemical formula of goethite is α-FeOOH, and they are commonly formed from iron-based minerals such as pyrite, magnetite, siderite, as well as iron-bearing silicate oxides through weathering processes. Goethite exhibits a diaspore structure, and the arrangement of oxygen and hydroxide ions follows a hexagonal close-packed pattern. Goethite displays various morphologies and is characterized by non-uniform sizes (Liu et al., 2013). The most fundamental form of goethite is acicular, with lengths ranging from tens of nanometers to a few microns.

Ferrihydrite and lepidocrocite are less commonly found in nature compared to goethite. Ferrihydrite appears as reddish-brown spherical nanoparticles, and its precise chemical formula is currently uncertain. The initial proposed composition is $Fe_5HO_8 \cdot 4H_2O$. Ferrihydrite is the primary sediment formed during the hydrolysis of Fe^{3+}. However, natural ferrihydrite is unstable and readily transforms into goethite or hematite over time. Due to its large surface area and high surface activity, ferrihydrite exhibits strong interactions through adsorption and coprecipitation processes, making it effective in pollutants removal from wastewater (Cismasu et al., 2011). Lepidocrocite, with a chemical composition of γ-FeO(OH), primarily originates from external sources and forms through the dehydration of iron hydroxide. It is rare

to find natural lepidocrocite in ore deposits. Currently, synthetic ferrihydrite and lepidocrocite are predominantly used for laboratory research purposes (Zhong et al., 2022; Chen et al., 2023b).

In addition to iron sulfide minerals and iron oxide minerals, siderite is another significant type of iron-based mineral known as an iron-bearing silicate mineral (Scheinost and Charlet, 2008). Natural siderite belongs to the trigonal crystal system, and its composition primarily consists of $FeCO_3$. Siderite is commonly found in granular, massive, or tuberculous forms. A notable advantage of siderite is that approximately 48.0% of its iron content does not contain sulfur or phosphorus, which gives it a considerable application advantage when compared to limonite, which contains only about 37.0% iron content.

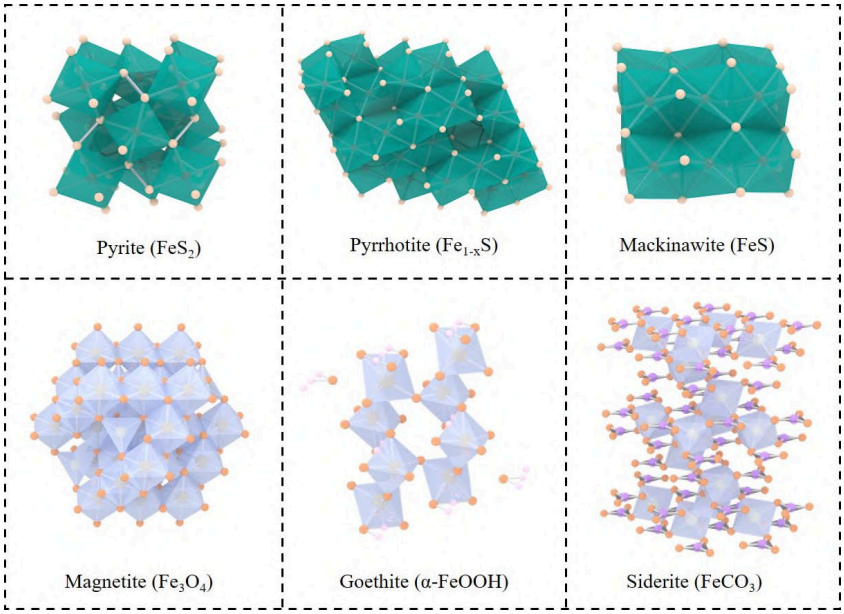


Fig. 3. The crystal structure of various iron-based minerals.

3.3 Bimetallic minerals

There are various bimetallic minerals that contain metallic elements such as Cu, V, Ti, Zn, and others. In comparison to monometallic catalysts, certain bimetallic oxides have been proven to exhibit superior catalytic performance in AOPs, including delafossite ($CuFeO_2$), copper ferrate ($CuFe_2O_4$), bismuth vanadate ($BiVO_4$), ferric vanadate ($FeVO_4$), and more (Chen et al., 2022b; Ding et al., 2016; Soufi et al., 2022; Zhang et al., 2021a). Studies have demonstrated that although these metal ions individually exhibit weak activation effects on HPO and PSs, the presence of bimetallic active sites can synergistically enhance catalytic performance, facilitating the Fe^{2+}/Fe^{3+} cycle in the reaction system and improving the degradation efficiency of organic pollutants. Moreover, copper minerals, magnesium minerals, and

titanium minerals are abundant on earth and possess the advantage of being inexpensive, similar to iron ore. Consequently, many researchers have become increasingly interested in exploring the potential of these bimetallic minerals for the removal of organic pollutants, leading to extensive research in this area.

There is a wide variety of copper minerals, with chalcopyrite and bornite being the primary copper minerals. Chalcopyrite ($CuFeS_2$) is the most prevalent copper ore. The crystal structure of chalcopyrite varies with temperature, typically crystallizing in the tetragonal system with the I-42d space group under normal temperature and pressure conditions (Barton and Hiskey, 2022). Its crystal structure is parallel to that of sphalerite, where Fe^{3+} and Cu^{+} substitute Zn^{2+} in tetrahedral sites and coordinate with sulfur ions, forming a copper-iron coordination tetrahedron structure. The Cu-S and Fe-S bonds exhibit characteristics of covalent bonding.

Bornite is another sulfide mineral that contains both copper and iron, similar to chalcopyrite. Its chemical formula is Cu_5FeS_4, and the reserves of bornite rank second only to chalcopyrite. Natural bornite exhibits three crystal types that vary with temperature. Under high temperature conditions, it adopts a cubic structure known as cubic-bornite. In this structure, six copper and iron atoms, along with two cation vacancies, are randomly distributed among eight sulfur tetrahedral active sites. At medium and low temperatures, bornite exhibits characteristics of cation orderliness and vacancy aggregation (Mikhlin et al., 2005). The iron atoms arrange in an orderly manner within the structure, coordinating with the surrounding atoms in the sulfur tetrahedron.

3.4 Multi-metal minerals

In natural magnetite, the presence of iron and transition metals often leads to isomorphic substitution. The doping of transition metal elements such as Ti, Cr, Co, and Mn into magnetite can influence the electron transfer rate between reactant surfaces, resulting in a significant enhancement of catalytic efficiency of magnetite (Costa et al., 2006; Khataee et al., 2018; Magalhães et al., 2007; Marsac et al., 2017). Several studies have indicated that V^{4+}/V^{5+} exhibits superior activation effects on PSs compared to other common transition metal catalysts such as Fe^{2+}/Fe^{3+}, Cu^{+}/Cu^{2+}, Mn^{2+}, and Ag^{+} (Fang et al., 2017). This may be attributed to the higher redox potential of V^{4+}/V^{5+} (0.99 V) in comparison to Fe^{2+}/Fe^{3+} (0.77 V), which indicates that vanadium species possess stronger activation capacity and are more prone to electron transfer reactions with oxidants, leading to the generation of reactive oxygen species (ROS) (Fang et al., 2018). The doping of transition metals into magnetite is primarily carried out through

synthesis in laboratory settings, thereby increasing the complexity of the experiments and the preparation costs.

Vanadium-titanium magnetite, a mineral naturally enriched with transition metals such as Fe, Ti, and V, serves as its primary component. This mineral maintains an inverse spinel-type structure, where V^{3+} and Ti^{4+} ions occupy octahedral sites (Liang et al., 2012). Additionally, natural vanadium-titanium magnetite exhibits magnetic properties, which facilitate the recovery of residual samples. However, it is crucial to acknowledge the strong toxicity of vanadium and exercise caution regarding the leaching of vanadium into the solution during waste disposal. The safe concentration limit for vanadium is only 0.33 $mg \cdot L^{-1}$.

There are natural minerals that contain little to no iron but still possess activating properties, with different catalytic mechanisms from iron minerals. Tourmaline belongs to a large group of cyclic annular silicate minerals and falls under the trigonal crystal system. The chemical structure of tourmaline is represented as $X_3Y_3Z_6T_6O_{18}(BO_3)_3W_3V$, where the X, Y, and Z sites typically accommodate metal cations such as Al^{3+}, Mg^{2+}, Fe^{2+}, Fe^{3+}, V^{3+}, and others. The T site corresponds to Si^{4+}, while the V site is occupied by OH^-, O^{2-}, and W can be OH^-, O^{2-}, or F^-. Tourmaline exhibits unique physicochemical properties including permanent spontaneous polarization, pyroelectricity, far-infrared radiation, and continuous release of anions, making it particularly useful in fields such as construction, textiles, and plastics (Liang et al., 2021). The permanent spontaneous polarization effect of tourmaline generates an electric field that can electrolyze water molecules to produce ·OH radicals. Due to its distinctive crystal structure, tourmaline creates a polarization charge at both ends of the crystal, forming an electrostatic field that attracts surrounding metal ions and impurities in a solution. This property makes it promising for application in sewage treatment and other related areas.

4. Natural minerals for heterogeneous AOPs

4.1 Iron sulfide minerals as catalysts

The degradation effects of natural iron sulfide minerals on pollutants are summarized in Table 1. Among these minerals, pyrite stands out as the most common heterogeneous catalyst. Its surface possesses abundant active reaction sites capable of degrading various organic pollutants. Research has shown that defect sites on the pyrite surface could generate ·OH radicals by water splitting, enabling the removal of pollutants through these active sites. Dhanasekara et al. discovered that natural pyrite could

remove 40.0% of carbofuran within 100 h without the presence of oxidants, and emphasized the role of sulfur species on the pyrite surface in the degradation process of carbofuran (Dhanasekara et al., 2015).

In the heterogeneous Fenton system, the decolorization rate of reactive orange 29 by pyrite was influenced by factors such as particle size, solution pH, initial concentration of H_2O_2 and reactive orange 29, as well as pyrite dosage (Khataee et al., 2016). Under the optimal conditions of initial orange 29 concentration 0.01 $g \cdot L^{-1}$, H_2O_2 3 mM, pyrite 3 $g \cdot L^{-1}$, and pH 2, a remarkable removal of 94.4% was obtained after 120 min. Furthermore, pyrite is capable of activating percarbonate to generate ·OH and $O_2^{\cdot-}$ radicals (Gu et al., 2023). The pyrite/sodium percarbonate system exhibited higher degradation efficiency for 1,2,3-trichloropropane compared to the traditional Fenton system. Within 240 min, while 1 mM H_2O_2 and 1 mM Fe^{2+} only removed 38.5% of 1,2,3-trichloropropane, a combination of 5 $g \cdot L^{-1}$ natural pyrite and 1 mM sodium percarbonate achieved a removal rate of 91.3%.

Compared to pyrite, natural pyrrhotite exhibits specific ferromagnetic properties, mainly attributed to the presence of iron vacancies (Lai et al., 2021). As the iron content increases, the magnetism gradually decreases. The ferromagnetic nature of natural pyrrhotite facilitates its easy separation and recovery after reactions, making it highly promising for wastewater treatment. Natural pyrrhotite can activate HPO and PSs to remove refractory pollutants from water. The activation effects of pyrrhotite on HPO and PSs varied under different pH conditions (Xia et al., 2017b). At pH of 3, pyrrhotite demonstrated a superior activation effect on PDS, as the pyrrhotite/PDS system achieved approximately 100.0% degradation of phenol within 20 min. In contrast, the degradation efficiency of phenol in the pyrrhotite/H_2O_2 system was only 59.0% within 30 min.

Apart from pH, studies have shown that chelating agents can affect the release of iron ions in solution. O-isopropyl-N-ethyl thionocarbamate (IPETC) acted not only as a pollutant but also as a chelating agent that bound to iron ions, allowing the leached iron ions from natural pyrrhotite to exist stably under neutral and near-neutral conditions (Wu et al., 2019). Additionally, ethylamine, an intermediate product of IPETC, could form organic radicals and promote the regeneration of Fe^{2+} during the activation of PDS. Fig. depicts the activation mechanism of natural pyrrhotite for PDS. Furthermore, studies have shown that the reaction between natural pyrrhotite and PDS could generate a charge transfer complex ($\equiv Fe^{2+}\cdots O_3SO\text{-}OSO_3^-$) that enhanced the production of ROS and facilitated the oxidation of *E. coli K-12* under aerobic conditions (Xia et al., 2017a). When 1 $g \cdot L^{-1}$ pyrrhotite and 1 mM PDS was added,

E. coli K-12 achieved an optimal inactivation rate of 7 $\log_{10}$ cfu·L^{-1} cells within 15 min. Apart from its ferromagnetic properties, natural pyrrhotite also exhibits electrical conductivity. The strong redox ability of Fe^{3+}/Fe^{2+} and S^{2-} renders pyrrhotite suitable as an electrode material and electrocatalyst in lithium-sulfur batteries (Wang et al., 2023a).

Mackinawite exhibits remarkable reactivity with various chemicals due to its chalcophilic affinity and strong reducing capacity (Jeong et al., 2008). Fan et al. compared the activation effects of zero-valent iron and natural mackinawite on PDS (Fan et al., 2018). Under similar conditions, the zero-valent iron/PDS system initially demonstrated a faster removal rate of total organic carbon (TOC), but the depletion of iron ions in zero-valent iron in the later stages led to a decrease in the removal rate. Conversely, the presence of S^{2-} on the surface of mackinawite better facilitated the Fe^{2+}/Fe^{3+} cycle and improved degradation efficiency. In addition, O_3 is a potent oxidant that effectively promotes the release of iron ions and further oxidizes Fe^{2+} (Peng et al., 2018). Natural mackinawite was introduced into a catalytic ozone oxidation to remove N, N-dimethylacetamide. Under optimized conditions, the degradation efficiency of N, N-dimethylacetamide in the natural mackinawite/O_3 system (95.4%) surpassed that of the zero-valent iron/O_3 system (46.1%) and synthetic FeS/O_3 system (68.8%). While mackinawite exhibits excellent catalytic performance, it has not yet been applied in heterogeneous Fenton systems. Additionally, its stability in the atmosphere may be a concern, which is why most current research involves synthesizing mackinawite rather than utilizing natural sources.

Natural minerals typically possess a relatively stable structure, resulting in low levels of iron ion leaching. While iron in solution can react with HPO and PSs, the production of ROS is limited, thereby impeding effective pollutant degradation. The activation mechanisms of iron sulfide minerals can be categorized as follows: (1) Fe^{2+}/Fe^{3+} on the mineral surface acts as active sites and reacts with oxidants to generate free radicals, as shown in Eq. 3-4 (Rahimi et al., 2021). (2) Minerals can undergo oxidation by oxidants. For instance, pyrite can react with O_2, H_2O_2, and PSs to yield iron ions, free radicals, and sulfur species (Eq. 5-7) (Chen et al., 2021a). Moreover, pyrite and mackinawite can serve as reducing agents, converting Fe^{3+} to Fe^{2+} (Eq. 8-9). (3) Sulfur ions present in iron sulfide minerals also play a crucial role in catalytic reactions by acting as electron donors that facilitate the regeneration of iron ions (Eq. 10-12).

$$Fe^{2+} + S_2O_8^{2-} \rightarrow SO_4^{\cdot-} + Fe^{3+} + SO_4^{2-} \quad (3)$$

$$Fe^{2+} + HSO_5^- \rightarrow SO_4^{\cdot-} + Fe^{3+} + OH^- \quad (4)$$

$$2FeS_2 + 7O_2 + 2H_2O \rightarrow 2Fe^{2+} + 4SO_4^{2-} + 4H^+ \quad (5)$$

$$2FeS_2 + 15H_2O_2 \rightarrow 2Fe^{3+} + 4SO_4^{2-} + 2H^+ + 14H_2O \quad (6)$$

$$FeS_2 + 2S_2O_8^{2-} \rightarrow 2SO_4^{\cdot-} + Fe^{2+} + 2SO_4^{2-} + 2S \quad (7)$$

$$FeS_2 + 14Fe^{3+} + 8H_2O \rightarrow 15Fe^{2+} + 2SO_4^{2-} + 16H^+ \quad (8)$$

$$FeS + 8Fe^{3+} + 4H_2O \rightarrow 9Fe^{2+} + SO_4^{2-} + 8H^+ \quad (9)$$

$$2Fe^{3+} + S^{2-} \rightarrow 2Fe^{2+} + S^0 \quad (10)$$

$$8Fe^{3+} + S^{2-} + 4H_2O \rightarrow 8Fe^{2+} + SO_4^{2-} + 8H^+ \quad (11)$$

$$14Fe^{3+} + S_2^{2-} + 4H_2O \rightarrow 14Fe^{2+} + 2SO_4^{2-} + 16H^+ \quad (12)$$

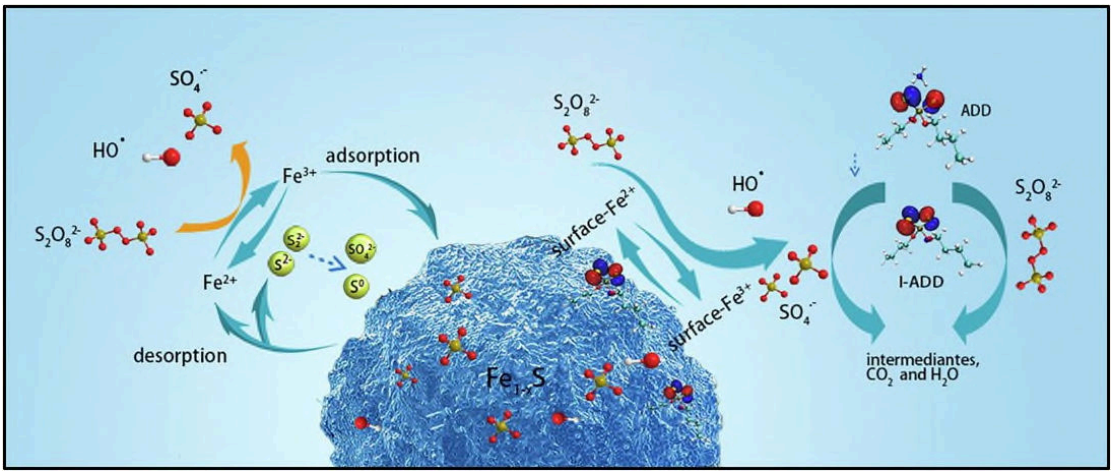


Fig. 4. The reaction mechanism of pyrrhotite activate PDS to remove ammonium dibutyl dithiophosphate. Reprinted with permission of Elsevier from Wu et al., 2020.

1 **Table 1.** The removal of organic pollutants by iron sulfide minerals in AOPs

Natural minerals	Organic pollutants	Oxidant concentration	Catalyst dosage	pH	Time	Removal efficiency	References
Pyrite	Reactive orange 29: 0.01 g·L^{-1}	H_2O_2: 3 mM	3 g·L^{-1}	2	120 min	94.4%	(Khataee et al., 2016)
Pyrite	Naphthalene: 0.1 mM	H_2O_2: 1 mM	2 g·L^{-1}	4	120 min	99.2%	(Yang et al., 2023b)
Pyrite	Nitrobenzene: 0.02 g·L^{-1}	H_2O_2: 250 mM	2 g·L^{-1}	3	300 min	80.0%	(Zhang et al., 2014)
Pyrite	COD: 0.16 g·L^{-1}	H_2O_2: 10 mM	24 g·L^{-1}	5	180 min	76.7%	(Chen et al., 2021a)
Pyrite	Methylene blue: 0.005 g·L^{-1}	H_2O_2: 9.97 M	2.5 mg	8	20 min	100.0%	(Wang et al., 2021c)
Pyrite	V(IV)-citrate: 0.4 mM	PMS: 5 mM	8 g·L^{-1}	3	180 min	99.4%	(Han et al., 2022)
Pyrite	Acetaminophen: 0.02 mM	PMS: 0.15 mM	1 g·L^{-1}	3	15 min	99.2%	(Wang and Dong, 2023)
Pyrite	Tetracycline: 0.05 g·L^{-1}	PMS: 1 g·L^{-1}	1 g·L^{-1}	4.1	30 min	98.3%	(Rahimi et al., 2021)
Pyrite	Imidacloprid: 0.001 mM	PDS: 1 mM	0.15 g·L^{-1}	3	60 min	98.9%	(Liu et al., 2023b)
Pyrite	Ethylthionocarbamate: 0.03 g·L^{-1}	PDS: 0.12 g·L^{-1}	1 g·L^{-1}	5	180 min	96.6%	(Chen et al., 2018)
Pyrite	Acid orange 7: 0.02 g·L^{-1}, Cr(VI): 0.01 g·L^{-1}	PDS: 0.4 g·L^{-1}	4 g·L^{-1}	2.5	60 min	100.0%	(Li et al., 2020)
Pyrite	Tris(2-chloroethyl) phosphate: 0.002 g·L^{-1}	PDS: 2.5 mM	0.15 g·L^{-1}	5	120 min	100.0%	(Lian et al., 2019)
Pyrite	COD: 0.79 g·L^{-1}	PDS: 12.5 mM	9.28 mM	6	1440 min	44.0%	(Sun et al., 2022a)

Pyrite	2,4-dichlorophenol: 0.03 $g \cdot L^{-1}$, Cr(VI): 0.02 $g \cdot L^{-1}$	PDS: 1 mM	1 $g \cdot L^{-1}$	5	120 min	76.2%, 80.1%	(He et al., 2021)
Pyrite	Microcystis aeruginosa: 3.5 (± 0.5) × 10^6 cells$\cdot mL^{-1}$	PDS: 1.2 mM	1 $g \cdot L^{-1}$	7	360 min	95.0%	(Zheng et al., 2022b)
Pyrite	COD: 0.94 $g \cdot L^{-1}$	PDS: 30 mM	1 $g \cdot L^{-1}$	5	720 min	82.0%	(Sun et al., 2022b)
Pyrrhotite	Ammonium dibutyl dithiophosphate: 0.04 $g \cdot L^{-1}$	PDS: 1 mM	0.35 $g \cdot L^{-1}$	7	180 min	100.0%	(Wu et al., 2020)
Pyrrhotite	*E. coli K-12*: 7 $\log_{10}$ cfu$\cdot mL^{-1}$	PDS: 0.5 mM	1 $g \cdot L^{-1}$	3	10 min	100.0%	(Xia et al., 2017a)
Pyrrhotite	O-isopropyl-N-ethyl thionocarbamate: 0.28 mM	PDS: 1.4 mM	0.7 $g \cdot L^{-1}$	6	150 min	100.0%	(Wu et al., 2019)
Pyrrhotite	Phenol: 0.02 mM	PDS: 0.5 mM	1.25 $g \cdot L^{-1}$	3	30 min	100.0%	(Xia et al., 2017b)
Mackinawite	P-chloroaniline: 0.2 mM	PDS: 4 mM	0.35 $g \cdot L^{-1}$	3	240 min	97.3%	(Fan et al., 2018)

2

4.2 Iron oxide minerals as catalysts

Table 2 presents the degradation effects of various natural iron oxide minerals on pollutants in AOPs. Compared to maghemite, magnetite, and hematite have received more research attention. Iron oxide minerals have been studied for reducing dissolved sulfide in water, remediating soil, and degrading organic pollutants (Zhang et al., 2016; Usman et al., 2012a; He et al., 2015; Usman et al., 2012b). Natural mesoporous hematite could act as a highly efficient PDS activator, capable of simultaneously degrading 2,4-dichlorophenoxyacetic acid and 2-methyl-4-chlorophenoxyacetic acid herbicides (Kermani et al., 2018). Under optimal conditions, the degradation efficiencies of both herbicides within 120 min were above 68.0%. Natural magnetite is primarily employed in heterogeneous Fenton systems, where it combined with H_2O_2 to adjust the pH of the Fenton reaction. At neutral pH, with a catalyst and oxidant dosage of 1 $g \cdot L^{-1}$, natural magnetite could completely remove sulfamethoxazole and mineralize aromatic intermediates into short-chain organic acids, achieved a mineralization rate of over 50.0% (Munoz et al., 2018). Furthermore, Wang and colleagues compared the degradation efficiency of azo dyes used different natural iron-bearing minerals in a heterogeneous Fenton system and found that while hematite exhibited superior adsorption capacity, magnetite demonstrated higher degradation efficiency for active yellow 3 compared to hematite and pyrite (Wang et al., 2022g).

The surface of natural goethite contains various types of ·OH groups, which is dependent on the coordination number of oxygen atoms and adjacent Fe^{3+} ions (Lai et al., 2021). The removal mechanism of goethite to bisphenol A is depicted in Fig. , wherein its abundant ·OH groups and high redox activity contribute to its significant potential in wastewater treatment. Goethite could serve as a catalyst in both H_2O_2 and PDS systems for the removal of bisphenol A (Ding et al., 2020). Within a duration of 240 min, the removal rates of bisphenol A in the respective systems were 75.9% and 61.4%. Notably, goethite exhibited a higher utilization rate of H_2O_2, which prevents the generation of excessive free radicals and their subsequent quenching.

Siderite has applications as an environmental mineral material for managing environmental pollution (Guo et al., 2007; Zhong et al., 2023). Fu and colleagues demonstrated the ability of siderite to remove methylene blue through adsorption and catalytic degradation. With 2.5 $g \cdot L^{-1}$ of sole siderite, approximately 50.0% of methylene blue was removed by adsorption. When 122.38 mM H_2O_2 was added at pH of 7, the removal efficiency of methylene blue reached 99.7% after 360 min (Fu et al., 2023). This

indicates that siderite can widen the range of pH applications and has a great degradation effect on different types of pollutants. Sun and colleagues used siderite as a catalyst for the heterogeneous Fenton reaction and found that the siderite/H_2O_2 system had an excellent degradation effect on bisphenol A, 2,4-dichlorophenoxyacetic acid, and sodium sulfadiazine, with degradation efficiencies of 54.0%, 44.0%, and 35.0%, respectively (Sun et al., 2021b). This is mainly because siderite can slowly release Fe^{2+} and activate H_2O_2 to produce ·OH in a pH range of 3 to 9. However, some studies have shown that methyl orange, which is also a dye, cannot be removed by the siderite/H_2O_2 system (Song et al., 2022). To remove methyl orange, Song and colleagues added persulfate to the reaction solution, created a binary oxidation system. When moderate persulfate was added, the degradation rate of methyl orange increased to nearly 100.0%, indicating that siderite also had a great activity effect on persulfate.

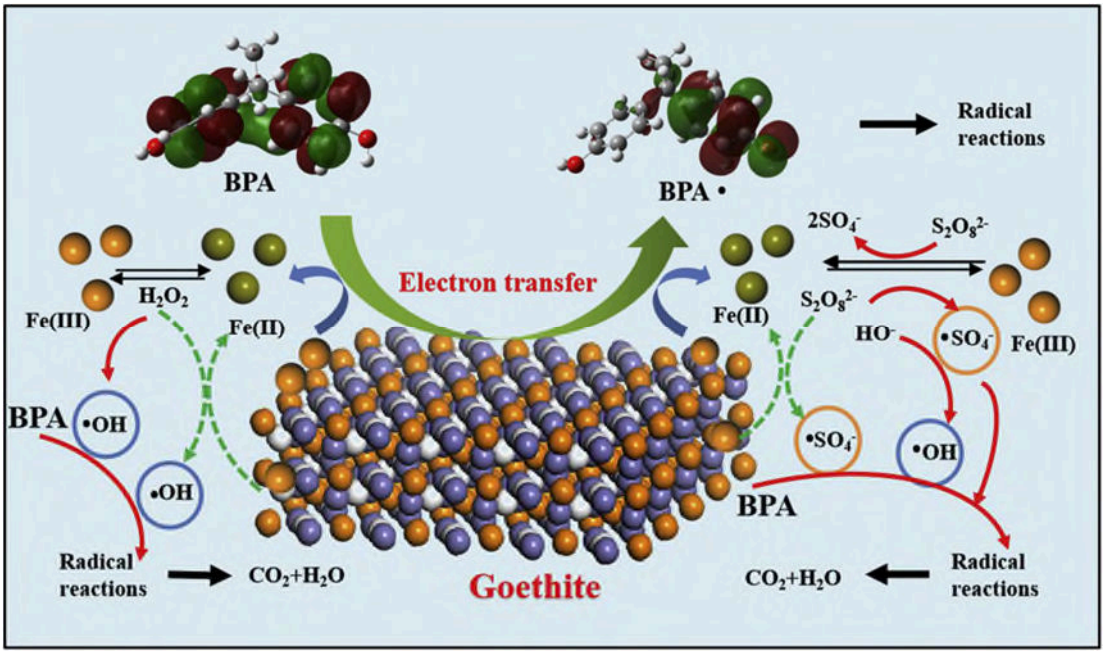


Fig. 5. The catalytic mechanism of goethite for bisphenol A removal. Reprinted with permission of Elsevier from Ding et al., 2020.

Table 2. The removal of organic pollutants by iron oxide minerals in AOPs.

Natural minerals	Organic pollutants	Oxidant concentration	Catalyst dosage	pH	Time	Removal efficiency	References
Goethite	Dimethyl sulphoxide: 1 g·L^{-1}	H_2O_2: 10 g·L^{-1}	100 g	5	360 min	76.8%	(Wu et al., 2006)
Goethite	Bisphenol A: 0.1 mM	H_2O_2: 1 mM	0.5 g·L^{-1}	3.5	240 min	87.6%	(Ding et al., 2020)
Hematite	Phenol: 0.1 mM	PMS: 1 mM	5 g·L^{-1}	3.3	60 min	100.0%	(Kang et al., 2021)
Hematite	2,4-dichlorophenoxyacetic acid: 0.5 g·L^{-1}, 2-methyl-4-chlorophenoxyacetic acid: 0.5 g·L^{-1}	PDS: 0.02 mM	0.5 g·L^{-1}	3	120 min	68.1%, 74.5%	(Kermani et al., 2018)
Magnetite	Sulfamethoxazole: 0.005 g·L^{-1}	H_2O_2: 0.025 g·L^{-1}	1 g·L^{-1}	5	240 min	100.0%	(Munoz et al., 2018)
Magnetite	Reactive yellow 3: 0.05 g·L^{-1}	H_2O_2: 0.5 mM	0.2 g·L^{-1}	3.5	40 min	100.0%	(Wang et al., 2022g)
Siderite	Carmine: 0.05 g·L^{-1}	[Siderite]/[H_2O_2] = 1:6	-	3	1440 min	99.9%	(Zhang et al., 2019)
Siderite	Methyl orange: 0.05 g·L^{-1}	H_2O_2: 60 mM, PDS: 2.5 mM	2.5 g·L^{-1}	7	720 min	100.0%	(Song et al., 2022)
Siderite	Sodium sulfadiazine: 10 mg·L^{-1}	H_2O_2: 100 mM	6 g·L^{-1}	3	90 min	98.0%	(Sun et al., 2020a)
Siderite	Sulfadiazine: 0.01 g·L^{-1}	PDS: 10 mM	1 g·L^{-1}	3	240 min	95.0%	(Sun et al., 2021a)
Siderite	2-chlorophenol: 0.334 mg·L^{-1}	PDS: 0.5 mM	0.05 g·L^{-1}	8.1	180 min	82.5%	(Zhong et al., 2023)
Siderite	Trichloroethene: 11.15 mM	H_2O_2: 150 mM, PDS: 6.3 mM	11.45 g·L^{-1}	3.01-2.66	1440 min	100.0%	(Yan et al., 2015)
Siderite	Trichloroethene: 11.15 mM	H_2O_2: 300 mM, PDS: 21 mM	0.1145 g	-	1440 min	100.0%	(Yan et al., 2013)
Siderite	Methylene blue: 0.1 g·L^{-1}	H_2O_2: 122.38 mM	2.5 g·L^{-1}	7	480 min	99.7%	(Fu et al., 2023)

4.3 Bimetallic minerals as catalysts

Table 3 provides the removal effects of various multi-metal minerals on organic pollutants. Chalcopyrite and bornite, as inexpensive and environmentally friendly natural catalysts, exhibit continuous release of Cu^{2+} and Fe^{2+} ions (Eq. 13-14). The presence of Cu^{+}/Cu^{2+} and Fe^{2+}/Fe^{3+} on the mineral surface activates HPO and PSs, while the reductive Cu^{+} facilitates the conversion of Fe^{3+} to Fe^{2+}. The synergistic action between Cu^{+} and Fe^{3+} enhances the reaction rate (Eq. 15-17). Furthermore, a redox cycle occurs between Cu^{+} and Fe^{3+}, with Cu^{+} reacting with dissolved oxygen to generate $O_2^{\cdot-}$ and promote pollutants degradation, as represented by Eq. 18-19 (Yang et al., 2022).

$$CuFeS_2 + 4O_2 \rightarrow Fe^{2+} + Cu^{2+} + 2SO_4^{2-} \quad (13)$$

$$CuFeS_2 + 8H_2O_2 \rightarrow Fe^{2+} + Cu^{2+} + 2SO_4^{2-} + 8H_2O \quad (14)$$

$$Cu^{+} + H_2O_2 \rightarrow Cu^{2+} + \cdot OH + OH^{-} \quad (15)$$

$$Cu^{2+} + H_2O_2 \rightarrow Cu^{+} + HO_2 \cdot + H^{+} \quad (16)$$

$$Cu^{+} + Fe^{3+} \rightarrow Cu^{2+} + Fe^{2+} \quad (17)$$

$$Cu^{+} + O_2 \rightarrow Cu^{2+} + O_2^{\cdot-} \quad (18)$$

$$Cu^{+} + O_2^{\cdot-} + 2H^{+} \rightarrow Cu^{2+} + H_2O_2 \quad (19)$$

In the system of natural chalcopyrite/PMS, the degradation efficiency of antibiotic sulfisoxazole reached 95.7% within 5 min, with a favorable degradation effect observed within the pH range of 3 to 6 (Zhou et al., 2022). To further investigate the activation mechanism of chalcopyrite, Xu and his team conducted Bader charge analysis used synthetic chalcopyrite and determined that iron on the surface serves as the primary catalytic active site during the activation process (Xu et al., 2019). Zhang et al. also reported similar findings, where Fe^{2+} demonstrated a superior activation effect compared to Fe^{3+}, Cu^{2+}, and Cu^{+} (Zhang et al., 2020b). Chalcopyrite, as a natural semiconductor mineral, can be further categorized into N-type and P-type (Huang et al., 2020). Fig. demonstrates the contribution of homogeneous and heterogeneous reaction systems in different types of chalcopyrite to removal the azo-dye orange II. N-type chalcopyrite exhibited a better removal effect on pollutants compared to P-type chalcopyrite, potentially due to the disparity in the released amount of Cu^{2+} between the two chalcopyrite types. Excessive copper ions can react with pollutants, forming intermediates and potentially quenching ·OH and $SO_4^{\cdot-}$ (Eq. 20-21), thereby negatively impacting degradation. Therefore, further investigations are necessary to understand the influence of metal ion leaching from chalcopyrite and

bornite on the reaction and the synergistic effects between Cu and Fe.

$$Cu^{+} + \cdot OH \rightarrow Cu^{2+} + OH^{-} \quad (20)$$

$$Cu^{+} + SO_4^{\cdot -} \rightarrow Cu^{2+} + SO_4^{2-} \quad (21)$$

Furthermore, these two natural minerals contain a significant number of sulfur. While sulfur is not the key component for activation, it plays a role as an electron donor, promoting the regeneration of Cu^{+}/Cu^{2+} and Fe^{2+}/Fe^{3+} (Eq. 22-24). Sulfur species could combine with protons on mineral surfaces, leading to the formation of sulfur vacancies (Yang et al., 2023a). This exposes more bimetallic active sites and increases the contact probability between active sites and reactants, thereby enhancing the activation capacity of chalcopyrite and bornite.

$$S^{2-} + Cu^{2+}/Fe^{3+} \rightarrow Cu^{+}/Fe^{2+} + S_2^{2-} \quad (22)$$

$$S_2^{2-} + Cu^{2+}/Fe^{3+} \rightarrow Cu^{+}/Fe^{2+} + S_n^{2-} \quad (23)$$

$$S_n^{2-} + Cu^{2+}/Fe^{3+} \rightarrow Cu^{+}/Fe^{2+} + SO_4^{2-} \quad (24)$$

Titanomagnetite, a constituent mineral of vanadium-titanium magnetite, contains $FeTiO_3$ and possesses potential catalytic properties. Lai and colleagues investigated the activation mechanism of titanomagnetite in the PMS system and discovered that Fe^{2+} and Fe^{3+} on the surface of titanomagnetite could generate high-valence iron-oxo species (Fe^{4+}=O and Fe^{5+}=O) through non-radical pathways, in addition to the conventional radical pathway (Lai et al., 2020). These high-valence iron-oxo species contribute to enhanced oxidation capabilities, potentially improving the degradation efficiency of organic pollutants. However, the production process and activation effect of high-valence iron species are not yet fully understood. Therefore, further research is necessary to investigate whether natural iron-bearing minerals can produce high-valence iron-oxo species during the activation process and to comprehend the underlying mechanisms.

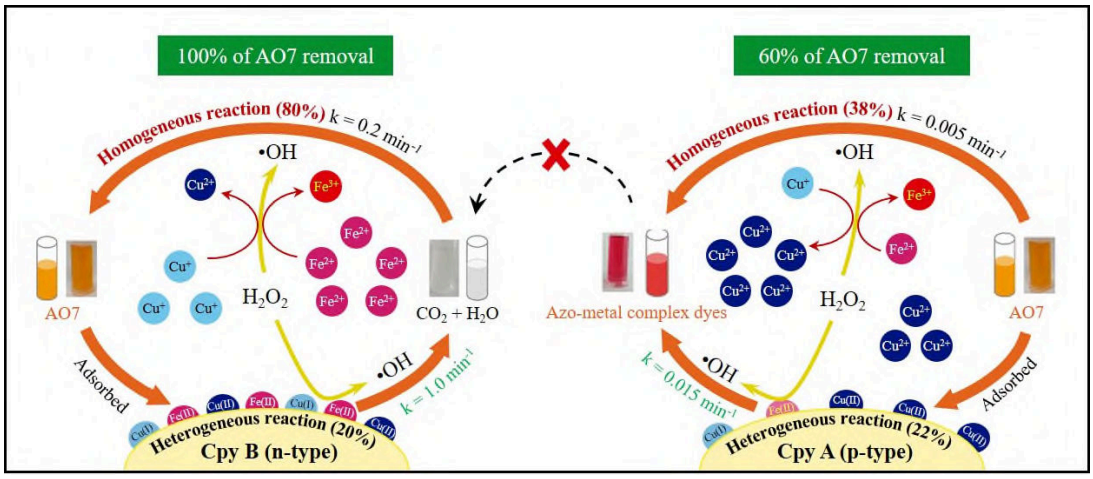


Fig. 6. The reaction mechanism of N-type and P-type chalcopyrite activate H_2O_2 to removal azo-dye. Reprinted with permission of Elsevier from Huang et al., 2020.

4.4 Multiple-metal minerals as catalysts

The catalytic effects of these less common natural minerals are summarized in Table 4. Natural vanadium-titanium magnetite exhibited a stronger catalytic effect on the decolorization of acid orange II in the heterogeneous Fenton system compared to magnetite, primarily due to the presence of vanadium and titanium (Liang et al., 2010). Natural vanadium-titanium magnetite was used to activate PMS for the degradation of bisphenol A and found that the vanadium-titanium magnetite/PMS system exhibited a wide pH application range (Lai et al., 2018). Irrespective of the initial pH, the degradation efficiency of bisphenol A exceeded 90.0% when vanadium-titanium magnetite was 12 $g \cdot L^{-1}$ and PMS was 4 mM.

Tourmaline can be classified into schorl, elbaite, and dravite based on the type of cations it contains. Wan et al. analyzed the catalytic effect of these three tourmalines and found that dissolved Fe^{2+} plays a key role in the activation process (Wen et al., 2022). However, in the reaction systems of elbaite and dravite, the pollutant tetracycline degraded mainly through non-free radical pathways, where tourmaline directly reacted with PDS to generate singlet oxygen ($^1O_2$). Moreover, due to electrolytic action, tourmaline may experience some metal ion loss, leading to the formation of electron-hole pairs to maintain electric neutrality. Studies have demonstrated that this defect could promote the generation of $^1O_2$, thereby enhanced the degradation rate (Zhang et al., 2021b). However, Yu and his team hold a different perspective on the activation mechanism of tourmaline with low iron content in the PMS system (Yu et al., 2020). The surface ·OH and structure ·OH groups could be replaced by the ·OH groups on HSO_5^-, which then combined with Al^{3+} to form aluminum hydroxy species, activated PMS. Consequently,

tourmaline exhibits remarkable catalytic efficiency and promising application prospects, but the activation mechanism remains unclear and requires further investigation.

Table 3 The removal rate of organic pollutants by multi-metal minerals in AOPs.

Natural minerals	Organic pollutants	Oxidant concentration	Catalyst dosage	pH	Time	Removal efficiency	References
Chalcopyrite	Sulfisoxazole: 0.005 g·L^{-1}	PMS: 0.5 mM	1 g·L^{-1}	3	15 min	99.3%	(Zhou et al., 2022)
Chalcopyrite	Carbamazepine: 0.005 g·L^{-1}	PMS: 0.5 g·L^{-1}	1 g·L^{-1}	6.67	30 min	82.3%	(Xi et al., 2023)
Chalcopyrite	Rhodamine B: 0.01 g·L^{-1}	H_2O_2: 39.2 mM	6 g·L^{-1}	5.2	120 min	96.5%	(Yang et al., 2022)
Chalcopyrite	Bisphenol S: 0.025 mM	PMS: 0.4 mM	2 g·L^{-1}	6.2	30 min	83.0%	(Peng et al., 2020)
Chalcopyrite	TOC: 0.156 g·L^{-1}	PMS: 25 mM	10 g·L^{-1}	8	120 min	71.0%	(Wang et al., 2022c)
Chalcopyrite	Rhodamine B: 0.1 g·L^{-1}	PDS: 0.002 g·L^{-1}	3 g·L^{-1}	6.5	1800 min	99.7%	(Zheng et al., 2022a)
Chalcopyrite	Azo-dye orange II: 0.1 g·L^{-1}	H_2O_2: 40 mM	2 g·L^{-1}	6.26	5 min	100.0%	(Huang et al., 2020)
Chalcopyrite	Tetracycline: 0.04 g·L^{-1}	H_2O_2: 40 mM	2 g·L^{-1}	-	100 min	86.4%	(Wang et al., 2022b)
Bornite	Tetracycline: 0.15 g·L^{-1}	PDS: 11.1 mM	3.5 g·L^{-1}	3.6 ± 0.1	180 min	81.6%	(Zhang et al., 2020b)
Bornite	Minocycline: 0.01 g·L^{-1}	H_2O_2: 0.5 mM	0.15 g·L^{-1}	4.5 ± 0.3	180 min	87.5%	(Yuan et al., 2021c)
Titanomagnetite	Atrazine: 0.01 g·L^{-1}	PDS: 5 mM	8 g·L^{-1}	6.3	90 min	92.0%	(Lai et al., 2020)

Table 4 The removal of organic pollutants by other natural minerals in AOPs.

Natural minerals	Organic pollutants	Oxidant concentration	Catalyst dosage	pH	Time	Removal efficiency	References
Tourmaline	Argazol blue: 0.2 g·L^{-1}	H_2O_2: 48.5 mM	10 g·L^{-1}	2	4 min	100.0%	(Xu et al., 2009)
Tourmaline	Methylene blue: 0.05 g·L^{-1}	H_2O_2: 0.1 mL	0.01 g	3	300 min	100.0%	(Wang et al., 2013)
Tourmaline	Methylene blue: 0.005 g·L^{-1}	PMS: 0.5 g·L^{-1}	1 g·L^{-1}	2.9	15 min	100.0%	(Yu et al., 2020)
Tourmaline	Sulfadiazine: 0.01 g·L^{-1}	PDS: 0.5 g·L^{-1}	0.5 g·L^{-1}	3	240 min	70.8%	(Niu et al., 2021)
Tourmaline	Sulfamethazine: 0.005 g·L^{-1}	PDS: 4 mM	5 g·L^{-1}	5	150 min	97.8%	(Zhang et al., 2021b)
Tourmaline	Tetracycline: 0.3 g·L^{-1}	PDS: 10 mM	1 g·L^{-1}	3	150 min	89.0%	(Wen et al., 2022)
Tourmaline	Tetracycline: 0.1 g·L^{-1}	H_2O_2: 9.9 mM	10 g·L^{-1}	3	600 min	95.2%	(Zhang et al., 2018)
Vanadium-titanium magnetite	Acid orange II: 0.2 mM	H_2O_2: 10 mM	1 g·L^{-1}	3	180 min	100.0%	(Liang et al., 2010)
Vanadium-titanium magnetite	Methyl orange: 0.05 g·L^{-1}	PDS: 12 mM	4 g·L^{-1}	3	120 min	99.7%	(Zhang et al., 2020a)
Vanadium-titanium magnetite	Bisphenol A: 0.05 g·L^{-1}	PMS: 4 mM	12 g·L^{-1}	6.4	120 min	90.0%	(Lai et al., 2018)

5. The influence of process factors

5.1 Effects of catalyst dosage and particle size

The concentration of active metal in the solution depends on the catalyst dosage. When pyrite in the Fenton system increased from 1 $g \cdot L^{-1}$ to 4 $g \cdot L^{-1}$, the rate constant of nitrobenzene degradation gradually increased (Zhang et al., 2014). Similarly, increased chalcopyrite from 0.5 $g \cdot L^{-1}$ to 1 $g \cdot L^{-1}$ improved the degradation efficiency of carbamazepine from 67.0% to 82.3% (Xi et al., 2023). They attributed this enhancement to the increased number of active sites, which promoted the activation of PMS to generate more ROS. However, there is an upper limit to the catalyst dosage. Exceeding the dosage does not further improve degradation efficiency and may even induce negative impacts. In the hematite/PDS system, the degradation efficiency of pollutants decreased when the hematite concentration exceeds 0.5 $g \cdot L^{-1}$, probably due to the quenching effect of excess Fe^{2+} produced by hematite on $SO_4^{\cdot-}$ (Kermani et al., 2018). In another study, the increased in schorl concentration from 10 $g \cdot L^{-1}$ to 15 $g \cdot L^{-1}$ resulted in minimal improvement in the decolorization rate of argazol blue (Xu et al., 2009). This limited enhancement may be attributed to the constraints imposed by H_2O_2 and pollutant concentrations, indicating that excessive catalyst usage can increase operational costs.

The particle size of natural minerals also plays a role in metal ion release. When the particle size of goethite increased from 70-80 mesh to 200-325 mesh, the concentration of Fe^{3+} increased from 1.0×10^{-6} M to 1.66×10^{-5} M, resulted in higher degradation efficiency for 2-chlorophenol (Lu, 2000). Similarly, as the particle size of pyrite particles decreased from 707 μm to 149 μm, the decolorization efficiency of reactive orange 29 in the heterogeneous Fenton system increased (Khataee et al., 2016). Furthermore, due to the spontaneous polarization of tourmaline, water molecules can be electrolyzed into ·OH, leading to the production of more free radicals as the particle size of tourmaline decreases (Zhang et al., 2018). Reducing the particle size of schorl from 100 μm to 15 μm significantly increased the removal rate of tetracycline in the schorl/H_2O_2 system due to the increase in active sites. However, when the particle size was further reduced, the reaction rate may slightly decrease. Regarding catalyst recovery and utilization, magnetic minerals with small particles can be easily recovered through magnetic field. However, the recovery and utilization of non-magnetic minerals is challenging.

5.2 Effects of oxidant dosage

The interaction between the dosage of catalyst and oxidant has a significant influence on

degradation, and the effect of oxidant dosage on degradation efficiency is similar to that of the catalyst dosage. In the siderite/H_2O_2 system, the degradation efficiency of methylene blue was directly proportional to the concentration of H_2O_2. When the H_2O_2 dosage increased from 24.48 mM to 734.25 mM, the removal rate of methylene blue increased by 32.0%, accompanied by an increase in the rate constant of the reaction (Fu et al., 2023).

However, it is worth noting that excessive concentrations of H_2O_2 can have a negative impact. In the study using goethite for methylene blue removal, excessive H_2O_2 reacted with ·OH, reducing the available ·OH species (Eq. 25-26) (Wang et al., 2015). A similar trend is observed in PSs systems, where an excess of $SO_4^{\cdot-}$ leads to self-quenching reactions, reducing the degradation efficiency of pollutants (Wang et al., 2022c). In the presence of surplus PMS or PDS, $SO_4^{\cdot-}$ can react to form $SO_5^{\cdot-}$, which possesses lower oxidizing ability (Eq. 27-28). Therefore, it is important to carefully optimize the dosage of both catalyst and oxidant to achieve optimal degradation efficiency while avoiding detrimental effects caused by excessive dosage.

$$H_2O_2 + \cdot OH \rightarrow HO_2^{\cdot} + H_2O \quad (25)$$

$$HO_2^{\cdot} + \cdot OH \rightarrow O_2 + H_2O \quad (26)$$

$$SO_4^{\cdot-} + SO_4^{\cdot-} \rightarrow S_2O_8^{2-} \quad (27)$$

$$SO_4^{\cdot-} + HSO_5^{-} \rightarrow SO_5^{\cdot-} + SO_4^{2-} + H^+ \quad (28)$$

Finding the optimal dosage of catalyst and oxidant is essential for application. On one hand, it ensures effective pollutants degradation. On the other hand, it helps reduce the consumption of chemicals, resulting in cost savings and improved economic benefits. The determination of optimal dosage involves a balance. Insufficient dosage of catalyst and oxidant may limit the degradation process, leading to incomplete pollutants removal. Conversely, excessive dosage can result in unnecessary chemical consumption, which not only increases operational costs but may also have adverse effects on the environment.

5.3 Effects of pH

The pH of the solution plays a critical role in catalytic reactions within heterogeneous HPO-based and PSs-based systems, impacting various levels of the catalytic process and influencing the presence of pollutants in the solution. Research has demonstrated that solution pH could influence the functional groups on the surface of goethite, resulted in an increase in the positively charged $FeOH^{2+}$ content on the

surface as the pH decreased (Wang et al., 2015). Wu et al. discovered that under neutral and alkaline conditions in the goethite/H_2O_2 system, dimethyl sulphoxide exhibited significant pollutants removal capabilities, likely due to changes in functional groups on the catalyst surface, thereby expanded its application range (Wu et al., 2006).

The pH also relates to the point of zero charge (pH_{pzc}) of materials (Peng et al., 2018). When the pH is lower than the pH_{pzc}, the ·OH groups on the catalytic surface undergo protonation, resulting in a positively charged catalyst surface. Conversely, when the pH exceeds the pH_{pzc}, deprotonation occurs, leading to a negatively charged catalyst surface, as depicted in Eq. 29-30. Tetracycline hydrochloride existed as a cation at pH levels below 3.3 and as an anion in alkaline environments (Kang et al., 2022; Wang et al., 2021d). In alkaline conditions, tetracycline experiences electrostatic repulsion with schorl, hindered its adsorption onto the catalyst surface. However, when the pH of the heterogeneous Fenton reaction was 12, natural pyrite could maintain a degradation rate of tetracycline above 55.0% (Mashayekh-Salehi et al., 2021). This suggests that electrostatic attraction or surface complexation is determined by the charge difference between the catalyst and pollutants surfaces at different pH values, and strong adsorption can promote pollutants degradation. Therefore, further investigation into the zero-point charge of different minerals and the behavior of pollutants at varying pH values is essential.

$$MOH + H^+ \leftrightarrow MOH_2^+ (pH < pH_{pzc}) \quad (29)$$

$$MOH + OH^- \leftrightarrow MO^- + H_2O (pH > pH_{pzc}) \quad (30)$$

While the utilization of natural minerals as heterogeneous catalysts can expand the pH range of reactions, it is generally observed that the removal rate of pollutants is higher under acidic and neutral conditions compared to alkaline conditions. In the pyrite/PMS system, the degradation efficiency of bisphenol S exhibited an inverse relationship with pH, gradually decreased from nearly 100.0% to approximately 70.0% as the pH increased from 3 to 11 (Peng et al., 2020). The high degradation efficiency observed in acidic conditions may be attributed to the conversion of PMS or PDS to $SO_4^{\cdot-}$ in an acidic environment, with the excess H_3O^+ ions further activated the metal active sites on the mineral surface, thereby accelerating the degradation process (Zheng et al., 2022a). Acidic conditions are not necessarily always optimal. In the pyrite/PMS system, a pH of 8 in the solution corresponded to the maximum removal rate of TOC (above 70.0%), while the removal rate of TOC declined under other pH conditions (Wang et al., 2022c). The high concentration of H^+ in a strong acid environment restrained

the hydrolysis of PMS, causing a decrease in the amount of $SO_4^{\cdot-}$, and certain anions present in the solution may impede the degradation process.

Under strong alkaline conditions, the leaching of Fe^{2+}/Fe^{3+} from minerals into the solution leads to their combination with OH^- ions, forming stable $Fe(OH)_2/Fe(OH)_3$ species (such as $FeOH^{2+}$, $Fe(OH_2)^+$, or $Fe(OH)_2^{4+}$) (Chen et al., 2018). These species can cover the surface of natural minerals, hindering the contact between oxidant and the active sites on the minerals surface. Interestingly, some non-iron-based minerals, such as dolomite and calcite, exhibit a weak dependency on pH. In alkaline conditions, these minerals can generate $^1O_2$ in addition to ·OH and $SO_4^{\cdot-}$, resulting in a high degradation efficiency (Zhang et al., 2022a). The pH of the solution has a significant impact on the types of free radicals formed. Peng and colleagues investigated the role of different radicals in the degradation process of the PMS system under varying initial pH conditions (Peng et al., 2020). They observed that ·OH and $SO_4^{\cdot-}$ played a major role in the degradation of bisphenol S under acidic and neutral conditions. However, under alkaline conditions, $S_2O_8^{2-}$ reacted with HO_2^- to generate a portion of $O_2^{\cdot-}$, which then transformed into $^1O_2$. The generation of various free radicals contributed to the enhanced degradation of pollutants (Eq. 31-32).

$$S_2O_8^{2-} + 2H_2O \rightarrow HO_2^- + 2SO_4^{2-} + 3H^+ \quad (31)$$

$$S_2O_8^{2-} + HO_2^- \rightarrow SO_4^{\cdot-} + SO_4^{2-} + H^+ + O_2^{\cdot-} \quad (32)$$

Therefore, although acidic conditions often exhibit high degradation efficiency, the optimal pH for pollutant removal depends on the specific system and should be determined to achieve the best performance. Solution pH has a profound influence on catalytic reactions, affecting surface properties of catalysts, altering the form of pollutants in solution, and influencing the adsorption and degradation processes. In-depth exploration of the relationship between pH, catalysts, and pollutants is crucial for advancing the understanding of the catalytic systems.

5.4 Effects of inorganic anions

When examining the treatment effectiveness of catalysts in real water environments, it is crucial to consider the presence of various inorganic anions, which are typically absent in simulated pollutant solutions. To explore the impact of these inorganic anions on catalytic reactions, numerous researchers have investigated their influence. Common inorganic anions found in water include Cl^-, CO_3^{2-}, HCO_3^-, NO_3^-, SO_4^{2-}, HPO_4^{2-}, and others (Wang and Wang, 2018b). However, the effects of these inorganic anions on catalytic reactions vary across different studies.

Cl^- is a common inorganic anion found in wastewater, and it often exerts an inhibiting effect on pollutant degradation (Zhang et al., 2020b). This is primarily due to the quench effect towards ·OH and $SO_4^{\cdot-}$, resulting in the generation of low redox potential species such as Cl·, $Cl_2^{\cdot-}$, $ClOH^{\cdot-}$, and Cl_2, as described by Eq. 33-38. However, several studies have indicated that the concentration of Cl^- significantly influences pollutant removal. For instance, in the mackinawite/PDS system, as the Cl^- concentration decreased from 100 mM to 1 mM, it gradually started to promote the degradation of 2,4-dichlorophenoxyacetic acid (Chen et al., 2017). Similarly, Liu et al. observed that Cl^- enhanced the degradation efficiency of imidacloprid in the pyrite/PDS system (Liu et al., 2023b). With an increase in Cl^- concentration from 0 to 0.5 mM, the removal rate of imidacloprid reached 95.9%. This enhancement could be attributed to the cooperative production of ·OH, Cl·, and high-valence iron species (Fe^{4+}) through the interaction of Fe^{2+} on the pyrite surface and HClO, as depicted in Eq. 39-41.

$$Cl^- + SO_4^{\cdot-} \rightarrow SO_4^{2-} + Cl^{\cdot} \quad (33)$$

$$Cl^- + \cdot OH \rightarrow ClOH^{\cdot-} \quad (34)$$

$$ClOH^{\cdot-} + H^+ \rightarrow Cl^{\cdot} + H_2O \quad (35)$$

$$Cl^- + Cl^{\cdot} \rightarrow Cl_2^{\cdot-} \quad (36)$$

$$Cl_2^{\cdot-} + Cl_2^{\cdot-} \rightarrow Cl_2 + 2Cl^- \quad (37)$$

$$Cl_2 + H_2O \rightarrow HClO + H^+ + Cl^- \quad (38)$$

$$Fe^{2+} + HClO \rightarrow Fe^{3+} + HO^{\cdot} + Cl^- \quad (39)$$

$$Fe^{2+} + HClO \rightarrow Fe^{3+} + HO^- + Cl^{\cdot} \quad (40)$$

$$Fe^{2+} + HClO \rightarrow FeO^{2+} + H^+ + Cl^- \quad (41)$$

Furthermore, SO_4^{2-} and NO_3^- are also common inorganic anions found in wastewater. In the pyrite/PMS system, NO_3^- had little influence on the degradation of tetracycline, whereas SO_4^{2-} significantly inhibited degradation (Rahimi et al., 2021). The presence of SO_4^{2-} hindered the decomposition of PMS and reduced the redox potential of $SO_4^{\cdot-}$. Similarly, Li and his colleagues found that NO_3^- and SO_4^{2-} had minimal effects on the reaction in the potassium persulfate system (Li et al., 2021b). However, NO_2^-, which is similar to NO_3^-, clearly inhibits the degradation process, as shown in Eq. 42. Nonetheless, some studies have indicated that NO_3^- could inhibit the formation of ·OH. When 10 mM of NO_3^- was added to the siderite/H_2O_2 system, the ·OH content was observed to decrease from 0.163 mM to 0.134 mM (Sun et al., 2021a). The inhibitory effect of NO_3^- is primarily attributed to the

formation of less active $NO_3^{\cdot}$ (2-2.2 V) through Eq. 43-44.

$$SO_4^{\cdot-} + NO_2^- \rightarrow SO_4^{2-} + NO_2 \quad (42)$$

$$NO_3^- + SO_4^{\cdot-} \rightarrow NO_3^{\cdot} + SO_4^{2-} \quad (43)$$

$$NO_3^- + \cdot OH \rightarrow NO_3^{\cdot} + OH^- \quad (44)$$

In the tourmaline/PDS system, $H_2PO_4^-$ had a stronger inhibitory effect on the degradation of sulfadiazine compared to Cl^- (Niu et al., 2021). On one hand, phosphate anions can act as quenching agents for ·OH and $SO_4^{\cdot-}$, and the production of OH^- can increase the solution pH. On the other hand, some studies have indicated that $HPO_4^{2-}/H_2PO_4^-$ had a strong affinity for the solid catalyst surface, leaded to the complexation with Fe^{2+}/Fe^{3+}, deactivation of surface-active sites, and a decrease in the leaching of metal ions.

Carbonate salts can increase the pH of the solution and maintain an alkaline reaction system. The addition of HCO_3^- to the tourmaline/PDS system increased the initial reaction pH from 5 to 9, promoted the degradation of sulfamethazine (Zhang et al., 2021b). This may be attributed to the transformation of $SO_4^{\cdot-}$ into ·OH, and studies have shown that $CO_3^{\cdot-}$ produced by the reaction between HCO_3^- and $SO_4^{\cdot-}$ exhibited high selectivity, thereby enhanced the pollutant removal. The inhibitory effect of CO_3^{2-}/HCO_3^- in AOPs involves two aspects. Carbonate ions quench ·OH, $SO_4^{\cdot-}$, and $O_2^{\cdot-}$ while generating other free radicals with lower oxidation reduction potential, and they also consume H^+ thereby hindering the release of Fe^{2+}/Fe^{3+} and reducing the degradation efficiency. It is evident that inorganic anions have both positive and negative effects on catalytic processes, highlighting the importance of carefully assessing their role in different reaction systems.

5.5 Effects of reaction temperature

In addition to active metal ions, thermal activation has also been found to activate H_2O_2 or PSs and generate ROS. The reaction temperature is an important factor in AOPs (Huang et al., 2022b). In studies on bacteria inactivation, an increase in temperature from 20 °C to 50 °C resulted in enhanced bacterial inactivation rates (Xia et al., 2017a). This is mainly attributed to the endothermic nature of the reaction between natural pyrrhotite and activated PDS, where higher temperatures promoted the generation of active radicals and accelerated the reaction rate. Moreover, increasing the temperature can lower the activation energy and enhance the rate of oxidation reactions. In the discoloration process of methyl orange, which was also an endothermic reaction, increased the temperature from 25 °C to 65 °C in the

vanadium-titanium magnetite/PDS system resulted in an increase in the discoloration rate from 91.4% to 99.7%, accompanied by a corresponding increase in the kinetic rate constant (Zhang et al., 2020a). Similarly, in the siderite/calcium sulfite system, only 10.0% of atrazine could be removed at 17 °C, whereas increased the temperature to 45 °C resulted in a degradation efficiency of atrazine exceeded 90.0% under the same conditions (Li et al., 2021a). Although higher temperatures are beneficial for pollutant degradation, maintaining the reaction system at elevated temperatures consumes significant energy. Additionally, excessively high temperatures can lead to the decomposition of H_2O_2, posing safety hazards during experiments. Therefore, it is favorable to operate catalytic process at room temperature.

6. Strategies for improving catalytic activity

6.1 External physical fields

Physical fields can be applied in AOPs to enhance catalytic efficiency. Light, electricity, ultrasound, and microwaves are commonly used to improve the removal of pollutants in the wastewater. Table 5 demonstrates pollutants removal by AOPs associated with natural minerals when different physical fields are introduced. Natural minerals such as pyrite, hematite, goethite, and ilmenite are excellent light-absorbing materials, which have been extensively studied in the field of photocatalysis. Pyrite, with its narrow band gap (0.95 eV), exhibited a strong light absorption ability and could be photoactivated to generate photoelectrons (e^-) and holes (h^+) (Guo et al., 2021; Zhang et al., 2022c). When light is utilized in the pyrite/Fenton system, the Fe^{3+}/Fe^{2+} cycle was significantly improved, and the complete oxidation time of p-nitrophenol was reduced from 10 min to 4 min (Zeng et al., 2019). Previous studies have highlighted the pH dependency of goethite during activation. To overcome this limitation, Shi and his team introduced visible light into the goethite/H_2O_2 system and observed the formation of highly selective $\equiv[Fe^{4+}O]^{2+}$ species under near-neutral pH conditions (Shi et al., 2023). At pH of 5, the photodegradation rate of cefradine could reach nearly 100.0%. In the case of iron oxide minerals, natural hematite serves as a semiconductor catalyst with a specific electronic band structure and a suitable optical band gap (2.1 eV) (Asif et al., 2021; Ni et al., 2022). Fig. a illustrates the reaction mechanism of hematite in photocatalytic reactions. When UV lamps were employed to irradiate the sulfite-activated hematite system, the degradation efficiency of metronidazole exceeded 92.0% within 5 min, given a sulfite/hematite molar ratio of 1:3 and a pH of 7.5 (Rasoulzadeh et al., 2023).

TiO_2 is a commonly used photocatalytic material, and researchers often combine it with other active

metals to synthesize new catalysts with improved photocatalytic properties. Ilmenite, a mineral abundant in Ti and Fe, has been recognized as a good photocatalyst, although there are limited reports on its activation of HPO or PSs. Numerous studies have demonstrated its efficacy as a photocatalyst due to its band gap ranging from 2.4 to 2.9 eV (Silveira et al., 2022; Zazo et al., 2020). Under the irradiation of a 3 $mW \cdot cm^{-2}$ white LED lamp, the ilmenite/PDS system not only generated $SO_4^{\cdot-}$ and ·OH radicals but also produced $^1O_2$ species in the reaction solution (Xia et al., 2018). Within 20 min, the ilmenite/PDS system completely inactivated *E. coli* with the involvement of a non-radical pathway. The presence of polymetallic ions in minerals exhibits a synergistic effect, significantly enhancing their photocatalytic abilities. Vanadium-titanium magnetite, similar to ilmenite, is rich in vanadium element. In a study by Liu et al., the synergistic interaction between ions in vanadium-titanium magnetite leaded to a reduction in the valence band potential and an increase in the charge transfer rate (Liu et al., 2022a). Additionally, the Ti-O bond and Fe-O-V bond provided electrons and accelerated the Fe^{2+}/Fe^{3+} cycle.

The introduction of an electric field in AOPs can enhance the oxidation capacity (Liu et al., 2023a). Several studies have demonstrated that heterogeneous electro-Fenton systems could facilitate the in-situ generation of H_2O_2, accelerate the Fe^{2+}/Fe^{3+} cycle, and reduce Fe^{3+} generated by the Fenton reaction to Fe^{2+} at the cathode (Eq. 45) (Barhoumi et al., 2017; Zeng et al., 2023). The reaction mechanisms of different iron ores in the electro-Fenton system are depicted in Fig. b. Among magnetite, siderite, hematite, and limonite, pyrite exhibited the most pronounced catalytic effect in the heterogeneous electro-Fenton system, achieved a paclitaxel removal rate of 99.1% when a current of 300 mA was applied (Hajiahmadi et al., 2022). Labiadh et al. employed chalcopyrite as a substitute for soluble iron salts in the traditional electro-Fenton system and found that the leaching of Fe^{3+} and Cu^{2+} from chalcopyrite induced synergistic effects (Labiadh et al., 2019). Cu^{2+} could react with H_2O_2 and radicals, or lose an electron at the cathode to produce Cu^+ (Eq. 46). Subsequently, Cu^{2+}/Cu^+ facilitated ·OH generation and Fe^{2+} regeneration.

$$Fe^{3+} + e^- \rightarrow Fe^{2+} \quad (45)$$

$$Cu^{2+} \rightarrow Cu^+ + e^- \quad (46)$$

Electric activation is an approach for activating persulfates, with electric current density being a crucial factor influencing electrochemical catalysis. A significant improvement in the degradation efficiency of acid orange 7 was observed in a natural maghemite/PDS system when the electric current

density increased from 0 to 150 $mA \cdot m^{-2}$ (Yan et al., 2017). This improvement was attributed to the promotion of Fe^{2+} formation and increased $SO_4^{\cdot-}$ production due to the higher current density. However, it is worth noting that higher current density is not necessarily. Excessively high current density can lead to the formation of H_2, which competes with Fe^{2+} for electrons (Lin et al., 2016).

Both ultrasound and microwave irradiation can provide a significant amount of energy to the reaction system, thereby facilitating the decomposition of H_2O_2 or PSs (Jiang et al., 2022a; Wang et al., 2023b). Ultrasound-assisted catalysis enhanced the adsorption process and accelerated the generation of free radicals at the bubble interface (Yu et al., 2014). Moreover, its cavitation effect exposes more active sites on the mineral surface. The reaction mechanism of microwave-assisted catalysis is illustrated in Fig. c. Under conditions of pyrite 1 $g \cdot L^{-1}$, PMS 2 mM, and pH 4.02, the degradation rate of 2,4-dichlorophenol reached 71.3% (Diao et al., 2020). However, ultrasound caused the increased leaching of iron ions in the solution and resulted in a 97.9% removal rate of 2,4-dichlorophenol. Furthermore, research has demonstrated that natural magnetite with microwave-absorbing properties facilitated the decomposition of PDS and enhanced the removal rate of p-nitrophenol in the magnetite/PDS system when exposed to microwave temperatures ranged from 60 °C to 80 °C (Hu et al., 2020).

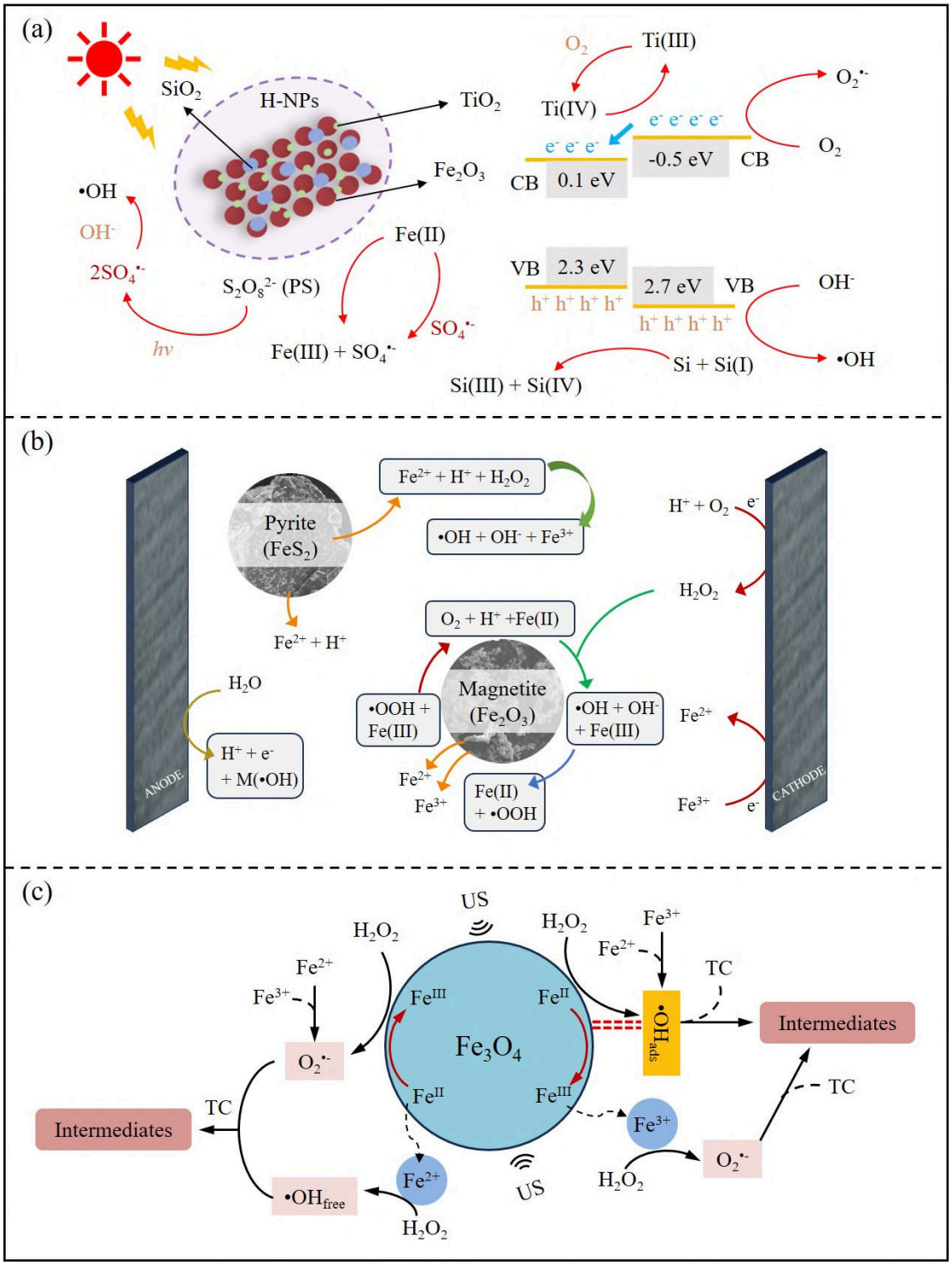


Fig. 7. (a) The possible photo-assisted reaction mechanism of hematite in PDS system. Reprinted with permission of Elsevier from Guo et al., 2022a. (b) The electro-Fenton reactions using different iron minerals. Reprinted with permission of Elsevier from Poza-Nogueiras et al., 2018. (c) The mechanism of ultrasound-assisted magnetite activation of H_2O_2. Reprinted with permission of Elsevier from Hou et al., 2016.

Table 5. The pollutants removal of natural minerals assisted by physical fields.

Physical fields	Natural minerals	Organic pollutants	Oxidant concentration	Assistance	pH	Time	Removal efficiency	References
Photo	Pyrite: 5 g·L^{-1}	Ofloxacin: 0.01 g·L^{-1}	H_2O_2: 1 mM	Light intensity: 15 kW·m^{-2}	3	180 min	94.7%	(Zhang et al., 2022c)
Photo	Pyrite: 3 g·L^{-1}	*E. coli*: 10^7 CFU·mL^{-1}	H_2O_2: 0.025 g·L^{-1}	Light intensity: 60 mW·cm^{-2}	7	30 min	100.0%	(Kalantary et al., 2019)
Photo	Goethite: 1 g·L^{-1}	Cefradine: 0.01 g·L^{-1}	H_2O_2: 5 mM	Halogen lamp: 400 W	5	480 min	100.0%	(Shi et al., 2023)
Photo	Goethite: 0.663 g·L^{-1}	Sulfamethoxazole: 0.001 g·L^{-1}	PDS: 419.3 mM	UVA: 500 W	-	319.8 min	100.0%	(Kanafin et al., 2023)
Photo	Hematite: 0.05 g·L^{-1}	Lomefloxacin: 0.01 g·L^{-1}	PMS: 0.8 mM	Xenon lamp: 35 W	5.98	120 min	82.0%	(Guo et al., 2022a)
Photo	Magnetite: 0.3 g·L^{-1}	Carbamazepine: 0.005 mM	H_2O_2: 0.5 mM	-	7.5	600 min	77.0%	(Gabet et al., 2023)
Photo	Siderite: 0.05 g·L^{-1}	4-Chlorophenol: 0.02 g·L^{-1}	H_2O_2: 2 ml	Light intensity: 930/13 μW·cm^{-2}	3	60 min	100.0%	(Bel Hadjltaief et al., 2018)
Photo	Chalcopyrite: 0.3 g·L^{-1}	Tetracycline: 0.03 g·L^{-1}	PMS: 0.3 g·L^{-1}	Xenon light	6	40 min	100.0%	(Yao et al., 2023)
Photo	Vanadium-titanium magnetite: 0.1 g·L^{-1}	Bisphenol S: 0.2 mM	PMS: 4 mM	Mercury lamp: 500 W	11	20 min	100.0%	(Liu et al., 2022a)
Photo	Ilmenite: 0.01 g·L^{-1}	*Enterococcus faecalis*: 10^6 CFU·mL^{-1}	PMS: 0.1 mM	Light intensity: 14 W·m^{-2}	7	120 min	100.0%	(García-Muñoz et al., 2022)
Photo	Basalt: 1 g·L^{-1}	Methylene blue: 0.07 g·L^{-1}	H_2O_2: 5 mM	Light intensity: 3.5 mW·cm^{-2}	2	60 min	100.0%	(Saleh et al., 2021)
Electricity	Pyrite: 2 g·L^{-1}	Tetracycline	PMS: 0.2 g·L^{-1}	Pulsed current: 200	4.2	120	91.0%	(Chen et al.,

		hydrochloride: 0.05 $g \cdot L^{-1}$		mA		min		2022a)
Electricity	Pyrite: 2 $g \cdot L^{-1}$	Tetracycline hydrochloride: 0.05 $g \cdot L^{-1}$	PMS: 0.1 $g \cdot L^{-1}$	Pulsed current: 100 mA	4.2	120 min	90.0%	(Chen et al., 2021b)
Electricity	Goethite: 0.5 $g \cdot L^{-1}$	Orange II: 0.05 $g \cdot L^{-1}$	PDS: 2 $g \cdot L^{-1}$	Current density: 8.4 $mA \cdot cm^{-2}$	7	120 min	92.1%	(Lin et al., 2016)
Electricity	Maghemite: 0.5 $g \cdot L^{-1}$	Acid orange 7: 0.05 mM	PDS: 100 mM	Current density: 100 $mA \cdot m^{-2}$	6	100 min	90.0%	(Yan et al., 2017)
Ultrasound	Pyrite: 1 $g \cdot L^{-1}$	2,4-dichlorophenol: 0.01 $g \cdot L^{-1}$	PMS: 2 mM	Ultrasonic power: 40 W	4.02	120 min	97.9%	(Diao et al., 2020)
Ultrasound	Magnetite: 1 $g \cdot L^{-1}$	Tetracycline: 0.1 $g \cdot L^{-1}$	PMS: 200 mM	Ultrasonic power: 80 W	3.7	90 min	89.0%	(Hou et al., 2012)
Ultrasound	Magnetite: 1 $g \cdot L^{-1}$	Tetracycline: 0.1 $g \cdot L^{-1}$	H_2O_2: 150 mM	Ultrasonic power: 80 W	3.7	60 min	93.6%	(Hou et al., 2016)
Ultrasound	Siderite: 0.75 $g \cdot L^{-1}$	Reactive yellow 81: 0.1 $g \cdot L^{-1}$	H_2O_2: 15 mM	Ultrasound: 40 KHz	3	30 min	88.6%	(Acisli et al., 2017)
Ultrasound	Tourmaline: 5 $g \cdot L^{-1}$	Bisphenol A: 0.005 $g \cdot L^{-1}$	H_2O_2: 50 mM	Ultrasonic power: 500 W (40 KHz)	2	120 min	98.7%	(Yu et al., 2014)
Microwave	Magnetite: 0.4 $g \cdot L^{-1}$	Rhodamine B: 0.3 $g \cdot L^{-1}$	H_2O_2/Mineralization ratio = 1	Microwave power: 500 W	2.4	7 min	100.0%	(Vieira et al., 2020)
Microwave	Magnetite: 2.5 $g \cdot L^{-1}$	P-nitrophenol: 0.02 $g \cdot L^{-1}$	PDS/PNP_{molar} = 15:1	Microwave temperature: 80 °C	3.4	28 min	94.2%	(Hu et al., 2020)

6.2 Adding reductants

As shown in Fig. , the degradation efficiency of natural minerals can be improved by adding reductants in addition to the external physical fields. In general, reductants with a redox potential lower than $E_0(Fe^{2+}/Fe^{3+})$ (0.771 V) can spontaneously reduce Fe^{3+} to Fe^{2+}, thereby enhancing the activation efficiency of oxidants and reducing the formation of iron sludge. Hydroxylamine (NH_2OH) is known for its strong reducibility and has been the focus of numerous studies in recent years. While hydroxylamine can directly react with peroxide as an electron donor, the reaction rate of direct activation is relatively slow (Duan et al., 2021). However, when metal ions or iron-containing materials are added, the activation efficiency of H_2O_2 or PSs can be significantly improved.

Hydroxylamine has been found to facilitate the regeneration of Fe^{2+} on the surface of pyrite, thereby enhanced electron transfer between pyrite and O_2 and increased the production of $HO_2^{\cdot}$ and $O_2^{\cdot-}$ (Huang et al., 2022a). The underlying mechanism of hydroxylamine promoting the reduction of Fe^{3+} can be described by Eq. 47-49 (Wang et al., 2021e). Hydroxylamine formed a complex with Fe^{3+} on the surface of pyrite and subsequently reduced it to Fe^{2+}. In the goethite/H_2O_2 system, the addition of hydroxylamine significantly increased the removal efficiency of alachlor from 6.0% to above 90.0%, suggesting the remarkable ability of hydroxylamine to enhance the degradation efficiency of heterogeneous Fenton systems (Hou et al., 2017).

$$Fe^{3+} + NH_2OH \rightarrow NH_2O\cdot + Fe^{2+} + H^+ \quad (47)$$

$$Fe^{3+} + NH_2O\cdot \rightarrow NHO + Fe^{2+} + H^+ \quad (48)$$

$$5Fe^{3+} + 2H_2O + NH_2O\cdot \rightarrow NO_3^- + 5Fe^{2+} + 6H^+ \quad (49)$$

In another study, the presence of hydroxylamine in the system increased the Fe^{2+} content on the surface of ilmenite, which played a crucial role in activating PDS (Yin et al., 2020). As the hydroxylamine concentration increased from 0.1 mM to 5 mM, the rate constant of ibuprofen degradation displayed a volcanic trend, with a low rate constant at higher concentrations, probably due to the quenching reaction of excess hydroxylamine on free radicals. Similar findings were reported by Sang et al., who investigated the use of transition metal oxides for sulfadiazine removal (Sang et al., 2020). Excessive hydroxylamine consumption of PMS and the capture of $SO_4^{\cdot-}$ and $\cdot OH$ to generate nitrogenous products were observed (Eq. 50-51). Wang and colleagues demonstrated that the addition of hydroxylamine in the copper tailings/hydroxylamine/PDS system resulted in higher continuous degradation efficiency of acid orange

7 (68.7%) compared to the copper tailings/PDS system (55.5%) (Wang et al., 2022d). This can be attributed to hydroxylamine's ability to accelerate the cycling of Fe^{2+}/Fe^{3+} and Cu^{+}/Cu^{2+} on the copper tailings' surface, thereby promoting the activation efficiency of PDS.

$$NH_2OH + \cdot OH \rightarrow OH^- + \text{nitrogenous products} \quad (50)$$

$$NH_2OH + SO_4^{\cdot-} \rightarrow SO_4^{2-} + \text{nitrogenous products} \quad (51)$$

In addition to hydroxylamine, other common reductants include ascorbate, thiosulfate, and sulfite. In the Fe^{2+}-activated PDS reaction, Wu et al. investigated the effects of different reductants and found that, apart from hydroxylamine, ascorbate had the most significant promoting effect on the degradation of trichloroethylene (Wu et al., 2015). Ascorbate ($C_6H_8O_6$) is a water-soluble vitamin commonly used as an antioxidant and chelating agent. Its strong reducing power makes it increasingly valuable in the environmental field. Ascorbate inhibits the conversion of H_2O_2 to O_2, thereby increasing the concentration of ·OH (Wang et al., 2021f). In a study by Wang et al., the addition of 1 mM ascorbate to the goethite/H_2O_2 system increased the accumulation of ·OH from 1.2 μmol to 6.6 μmol, significantly enhanced the utilization rate of H_2O_2. Furthermore, in the presence of 0.5 mM ascorbate, 1 $g \cdot L^{-1}$ magnetite, 1 mM H_2O_2, and an initial pH of 4, the removal rate of alachlor reached 69.5% within 20 min (Sun et al., 2020b). These examples demonstrate that the addition of a reductant can effectively enhance the removal efficiency of pollutants.

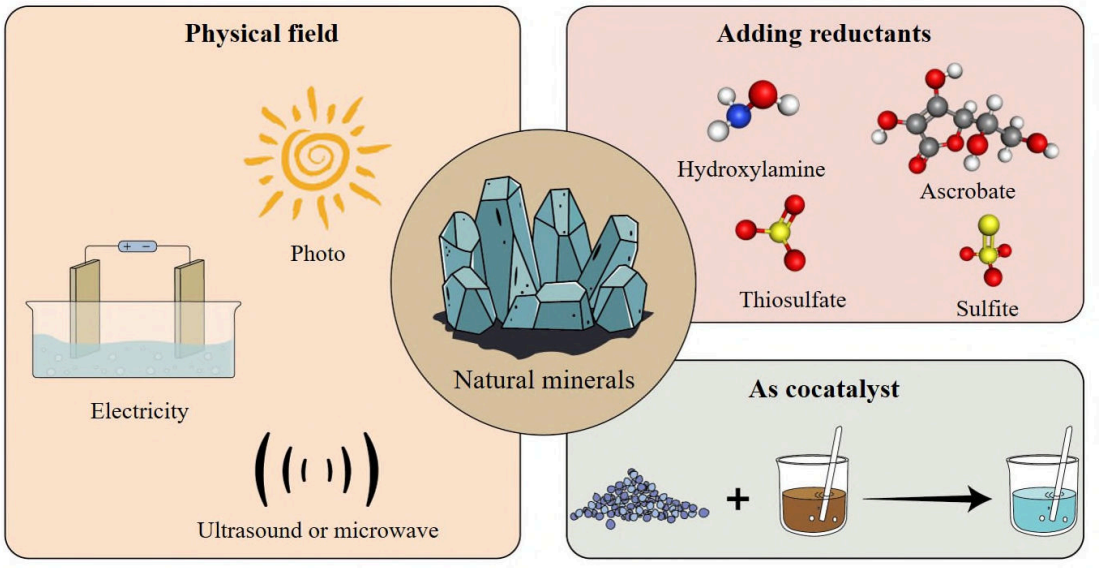


Fig. 8. Several strategies to improve the catalytic capacity of natural minerals.

6.3 Minerals as cocatalyst

Apart from their use as catalysts, natural minerals can also serve as cocatalysts. The degradation

efficiency of pollutants using different types of clay minerals is closely related to the content of surface and structural hydroxyl groups present in these minerals (Li et al., 2019). Due to the relatively low content of ·OH groups between montmorillonite layers, the degradation efficiency of atrazine in a PMS system was only 20.0%. However, montmorillonite possesses a large specific surface area and strong adsorption capacity. Wang et al. enriched the natural montmorillonite layers with Fe^{3+} through cation exchange and utilized the unique layered structure of montmorillonite to facilitate electron transfer, thereby promoting the Fe^{2+}/Fe^{3+} cycle and micropollutant removal (Wang et al., 2020).

Natural chalcocite, a copper sulfide mineral with the chemical formula Cu_2S, exhibits poor activation effects on peroxide. Due to the potential environmental harm associated with significant leaching of copper ions, chalcocite was primarily used as a cocatalyst to enhance the generation rate of Fe^{2+} free radicals in conjunction with Fe^{2+} (Yuan et al., 2021b). It is crucial to control the amount of Fe^{2+} and the leaching rate of copper ions when using chalcocite as a cocatalyst. To prevent excess copper ions from quenching free radicals, the addition of a moderate amount of chalcocite to limit the leaching rate of Cu^{+} can be an effective approach.

Additionally, several studies have demonstrated that molybdenite, which natural mineral rich in defects, possesses highly reducible Mo^{4+} ions. While the direct activation effect of natural molybdenite on H_2O_2 was poor, the defects on its surface provided a significant number of active Mo^{6+} sites (Yuan et al., 2021a). Taking advantage of this, Jiang and his team utilized natural molybdenite as a cocatalyst in the Fenton reaction (Jiang et al., 2021). They observed that H_2O_2 could react with Mo^{6+} on the molybdenite surface, generated Mo^{5+} and facilitated a redox cycle between Fe^{2+}/Fe^{3+} and Mo^{5+}/Mo^{6+}. This approach substantially improved the degradation efficiency of the Fenton system. Considering the potential harm posed by molybdenum ions in molybdenite, Li et al. aimed to enhance the degradation efficiency of the heterogeneous Fenton reaction (Li et al., 2022). They introduced pyrite as a cocatalyst to enhance the catalytic activity of Fe^{3+}. The addition of $1 g \cdot L^{-1}$ pyrite to a solution contained Fe^{3+} and PMS increased the rate constant of sulfamethoxazole degradation by over five times, indicating the synergistic activation of PMS by pyrite and Fe^{3+}.

7. Research perspectives

The significant application potential of natural minerals as heterogeneous catalysts has been summarized. However, several aspects require further attention in research and application.

a) Synthetic catalysts typically consist of single pure chemical substances, whereas natural minerals contain numerous metallic elements influenced by formation conditions. During the activation process, the leaching of these metal ions can vary, potentially impacting pollutants degradation. Hence, prior to experimentation, it is crucial to identify the type and concentration of leached active metals and assess their potential effects on catalytic reactions and secondary pollution.

b) Previous studies have emphasized the crucial role of high-valence metal ions (such as Fe^{4+}, Cu^{3+}, Mo^{5+}) and intermediate reactants in the activation process. Defects like oxygen and sulfur vacancies also offer additional active sites that facilitate pollutants degradation. However, a definitive understanding regarding the presence of high-valence metal ions in different oxidation systems and the contribution of defects to pollutants degradation is currently lacking. Therefore, future research on catalytic mechanisms should examine the role of high-valence metal ions and the regulation of defects.

c) In addition to the technological factors mentioned above, such as catalyst dosage, oxidant concentration, and pH, the dissolved oxygen also affects pollutants removal. This is primarily because Fe^{2+} reacts with O_2 in the solution, forming $O_2^{\cdot-}$. Furthermore, natural organic compounds are commonly present in water, and their quinone or quinoid groups may influence peroxide activation.

d) While external physical fields are effective in enhancing degradation efficiency, long-term energy output inevitably increases operational costs. Therefore, future research and application may still be subject to equipment and environmental constraints.

e) Currently, modification methods such as high temperature activation and mechanical ball milling have been employed for natural mineral treatment. There is still requirement of developing efficient and cheap modification methods for improving the catalytic performance of natural minerals.

8. Conclusions

Natural minerals exhibit great potential as heterogeneous catalysts for pollutants degradation. Natural minerals offer diverse metallic elements and surface defects that play crucial roles in the activation process. Natural iron-based minerals are still the main choice for future research due to their high catalytic activity of iron ion, non-toxic and rich mineral types and reserves. In the process of pollutant removal using natural minerals, it is mainly affected by catalyst dosage, oxidant dosage, pH

and temperature. Solution pH will not only affect the leaching of metal ions during the reaction, but also change catalytic surface properties and the existence form of pollutants in solution. Due to the large number of impurities in natural minerals, the catalytic activity is relatively low. And that external physical field can provide additional energy input to the reaction system and promote the activation of H_2O_2 and PSs. Further investigations are required for advancing the understanding and optimizing the application of natural minerals as catalysts in wastewater treatment. Future research should pay more attention to metal leaching, high-valence metal species, defects in minerals, dissolved oxygen, natural organic compounds, external physical fields, and modification methods of natural minerals.

Competing Interests

The authors have no conflicts to declare.

Credit Author Statement

Hongwen Liu led the literature collection and the writing of the manuscript; Xingyang Li and Xiuxiu Zhang contributed to the literature analysis. Frederic Coulon and Chongqing Wang contributed to the writing and revision of the manuscript. All authors agreed with the submission of the manuscript.

References

Acisli, O., Khataee, A., Darvishi Cheshmeh Soltani, R., and Karaca, S. (2017). Ultrasound-assisted Fenton process using siderite nanoparticles prepared via planetary ball milling for removal of reactive yellow 81 in aqueous phase. Ultrason Sonochem, 35, 210–218. https://doi.org/10.1016/j.ultsonch.2016.09.020

Andrews, C. B., & Hennet, R. J. (2022). Quest for groundwater quality sustainability–lessons from 40 years of remediation in the United States. Sustainable Horizons, 2, 100009. https://doi.org/10.1016/j.horiz.2022.100009

Ashraf, M., Khan, I., Usman, M., Khan, A., Shah, S. S., Khan, A. Z., Saeed, K., Yaseen, M., Ehsan, M. F., Tahir, M. N., and Ullah, N. (2020). Hematite and Magnetite Nanostructures for Green and Sustainable Energy Harnessing and Environmental Pollution Control: A Review. Chem Res Toxicol, 33(6), 1292–1311. https://doi.org/10.1021/acs.chemrestox.9b00308

Asif, A. H., Wang, S., and Sun, H. (2021). Hematite-based nanomaterials for photocatalytic degradation of pharmaceuticals and personal care products (PPCPs): A short review. Curr Opin Green Sustain Chem, 28, 100447. https://doi.org/10.1016/j.cogsc.2021.100447

Barhoumi, N., Olvera-Vargas, H., Oturan, N., Huguenot, D., Gadri, A., Ammar, S., Brillas, E., and Oturan, M. A. (2017). Kinetics of oxidative degradation/mineralization pathways of the antibiotic tetracycline by the novel heterogeneous electro-Fenton process with solid catalyst chalcopyrite. Appl Catal B, 209, 637–647. https://doi.org/10.1016/j.apcatb.2017.03.034

Barton, I. F., and Hiskey, J. B. (2022). Chemical, crystallographic, and electromagnetic variability in natural chalcopyrite and implications for leaching. Miner Eng, 189, 107867. https://doi.org/10.1016/j.mineng.2022.107867

Bel Hadjltaief, H., Sdiri, A., Gálvez, M. E., Zidi, H., Da Costa, P., and Ben Zina, M. (2018). Natural Hematite and Siderite as Heterogeneous Catalysts for an Effective Degradation of 4-Chlorophenol via Photo-Fenton Process. Chem Engineering, 2(3), Article 3. https://doi.org/10.3390/chemengineering2030029

Chen, H., Zhang, Z., Feng, M., Liu, W., Wang, W., Yang, Q., and Hu, Y. (2017). Degradation of 2,4-dichlorophenoxyacetic acid in water by persulfate activated with FeS (mackinawite). Chem Eng J, 313, 498–507. https://doi.org/10.1016/j.cej.2016.12.075

Chen, S., Xiong, P., Zhan, W., and Xiong, L. (2018). Degradation of ethylthionocarbamate by pyrite-activated persulfate. Miner Eng, 122, 38–43. https://doi.org/10.1016/j.mineng.2018.03.022

Chen, Q., Yao, Y., Zhao, Z., Zhou, J., and Chen, Z. (2021a). Long term catalytic activity of pyrite in Heterogeneous Fenton-like oxidation for the tertiary treatment of dyeing wastewater. J Environ Chem Eng, 9(4), 105730. https://doi.org/10.1016/j.jece.2021.105730

Chen, X., Han, Y., Gao, P., and Li, H. (2021b). New insight into the mechanism of electro-assisted pyrite minerals activation of peroxymonosulfate: Synergistic effects, activation sites and electron transfer. Sep Purif Technol, 274, 118817. https://doi.org/10.1016/j.seppur.2021.118817

Chen, X., Zhao, N., and Hu, X. (2022a). A novel strategy of pulsed electro-assisted pyrite activation of peroxymonosulfate for the degradation of tetracycline hydrochloride. Sep Purif Technol, 280, 119781. https://doi.org/10.1016/j.seppur.2021.119781

Chen, Z., Mi, N., Huang, L., Wang, W., Li, C., Teng, Y., and Gu, C. (2022b). Snow-like BiVO4 with rich oxygen defects for efficient visible light photocatalytic degradation of ciprofloxacin. Sci Total Environ, 808, 152083. https://doi.org/10.1016/j.scitotenv.2021.152083

Chen, S., Zhu, M., Guo, X., Yang, B., and Zhuo, R. (2023a). Coupling of Fenton reaction and white rot

fungi for the degradation of organic pollutants. Ecotoxicol Environ Saf, 254, 114697. https://doi.org/10.1016/j.ecoenv.2023.114697

Chen, X., Gu, X., Wang, C., Huang, L., Wu, D., Wu, H., Liang, S., Ling, J., and Gu, C. (2023b). Bisulfite-assisted surface Fenton-like degradation of dimethyl phthalate by ferrihydrite-H2O2 system. Chem Eng J, 452, 139309. https://doi.org/10.1016/j.cej.2022.139309

Cismasu, A. C., Michel, F. M., Tcaciuc, A. P., Tyliszczak, T., and Brown, J., Gordon E. (2011). Composition and structural aspects of naturally occurring ferrihydrite. C R Geosci, 343(2), 210–218. https://doi.org/10.1016/j.crte.2010.11.001

Costa, R. C. C., Lelis, M. F. F., Oliveira, L. C. A., Fabris, J. D., Ardisson, J. D., Rios, R. R. V. A., Silva, C. N., and Lago, R. M. (2006). Novel active heterogeneous Fenton system based on Fe3−xMxO4 (Fe, Co, Mn, Ni): The role of M2+ species on the reactivity towards H2O2 reactions. J Hazard Mater, 129(1), 171–178. https://doi.org/10.1016/j.jhazmat.2005.08.028

Dolatabadi, M., Ghaneian, M. T., Wang, C., & Ahmadzadeh, S. (2021). Electro-Fenton approach for highly efficient degradation of the herbicide 2, 4-dichlorophenoxyacetic acid from agricultural wastewater: Process optimization, kinetic and mechanism. J Mol Liq, 334, 116116. https://doi.org/10.1016/j.molliq.2021.116116

Dolatabadi, M., Świergosz, T., Wang, C., & Ahmadzadeh, S. (2023). Accelerated degradation of groundwater-containing malathion using persulfate activated magnetic Fe3O4/graphene oxide nanocomposite for advanced water treatment. Arab J Chem, 104424. https://doi.org/10.1016/j.arabjc.2022.104424

Dhanasekara, S. A. K. M., Attanayake, A. N. B., Herath, A. C., Nanayakkara, N., Senaratne, A., Indrarathne, S. P., and Weerasooriya, R. (2015). Partial degradation of carbofuran by natural pyrite. Environ Nanotechnol Monit Manag, 4, 51–57. https://doi.org/10.1016/j.enmm.2015.07.002

Diao, Z.-H., Lin, Z.-Y., Chen, X.-Z., Yan, L., Dong, F.-X., Qian, W., Kong, L.-J., Du, J.-J., and Chu, W. (2020). Ultrasound-assisted heterogeneous activation of peroxymonosulphate by natural pyrite for 2,4-diclorophenol degradation in water: Synergistic effects, pathway and mechanism. Chem Eng J, 389, 123771. https://doi.org/10.1016/j.cej.2019.123771

Ding, Y., Tang, H., Zhang, S., Wang, S., and Tang, H. (2016). Efficient degradation of carbamazepine by easily recyclable microscaled CuFeO2 mediated heterogeneous activation of peroxymonosulfate. J

Hazard Mater, 317, 686–694. https://doi.org/10.1016/j.jhazmat.2016.06.004

Ding, J., Shen, L., Yan, R., Lu, S., Zhang, Y., Zhang, X., and Zhang, H. (2020). Heterogeneously activation of H2O2 and persulfate with goethite for bisphenol A degradation: A mechanistic study. Chemosphere, 261, 127715. https://doi.org/10.1016/j.chemosphere.2020.127715

Duan, J., Pang, S., Wang, Z., Zhou, Y., Gao, Y., Li, J., Guo, Q., and Jiang, J. (2021). Hydroxylamine driven advanced oxidation processes for water treatment: A review. Chemosphere, 262, 128390. https://doi.org/10.1016/j.chemosphere.2020.128390

Dutt, M. A., Hanif, M. A., Nadeem, F., and Bhatti, H. N. (2020). A review of advances in engineered composite materials popular for wastewater treatment. J Environ Chem Eng, 8(5), 104073. https://doi.org/10.1016/j.jece.2020.104073

Elmacı, G., Özgenç, G., Kurz, P., & Zumreoglu-Karan, B. (2020). Enhanced water oxidation performances of birnessite and magnetic birnessite nanocomposites by transition metal ion doping. Sustainable Energy & Fuels, 4(6), 3157-3166. https://doi.org/10.1039/D0SE00301H

Elmacı, G. (2020). Magnetic hollow biocomposites prepared from Lycopodium clavatum pollens as efficient recyclable catalyst. ChemistrySelect, 5(7), 2225-2231. https://doi.org/10.1002/slct.201904152

Elmaci, G., Frey, C. E., Kurz, P., & Zumreoglu-Karan, B. (2015). Water oxidation catalysis by birnessite@ iron oxide core–shell nanocomposites. Inorganic Chemistry, 54(6), 2734-2741. https://doi.org/10.1021/ic502908w

Fan, J., Gu, L., Wu, D., and Liu, Z. (2018). Mackinawite (FeS) activation of persulfate for the degradation of p-chloroaniline: Surface reaction mechanism and sulfur-mediated cycling of iron species. Chem Eng J, 333, 657–664. https://doi.org/10.1016/j.cej.2017.09.175

Fan, B. Y., Liu, H. B., Wang, Z. H., Zhao, Y. W., Yang, S., Lyu, S. Y., ... & Liu, X. Y. (2021). Ferroelectric polarization-enhanced photocatalytic performance of heterostructured BaTiO3@ TiO2 via interface engineering. Journal of Central South University, 28(12), 3778-3789. https://doi.org/10.1007/s11771-021-4847-y

Fang, G., Wu, W., Deng, Y., and Zhou, D. (2017). Homogenous activation of persulfate by different species of vanadium ions for PCBs degradation. Chem Eng J, 323, 84–95. https://doi.org/10.1016/j.cej.2017.04.092

Fang, G., Deng, Y., Huang, M., Dionysiou, D. D., Liu, C., and Zhou, D. (2018). A mechanistic

understanding of hydrogen peroxide decomposition by vanadium minerals for diethyl phthalate degradation. Environ Sci Technol, 52(4), 2178–2185. https://doi.org/10.1021/acs.est.7b05303

Frison, R., Cernuto, G., Cervellino, A., Zaharko, O., Colonna, G. M., Guagliardi, A., and Masciocchi, N. (2013). Magnetite–Maghemite Nanoparticles in the 5–15 nm Range: Correlating the Core–Shell Composition and the Surface Structure to the Magnetic Properties. A Total Scattering Study. Chem Mater, 25(23), 4820–4827. https://doi.org/10.1021/cm403360f

Fu, C., Yan, M., Wang, Z., Li, J., Zhang, X., Song, W., Xu, Z., Bhatt, K., Wang, Z., and Zhu, S. (2023). New insights into the degradation and detoxification of methylene blue using heterogeneous-Fenton catalyzed by sustainable siderite. Environ Res, 216, 114819. https://doi.org/10.1016/j.envres.2022.114819

Gabet, A., Guy, C., Fazli, A., Métivier, H., de Brauer, C., Brigante, M., and Mailhot, G. (2023). The ability of recycled magnetite nanoparticles to degrade carbamazepine in water through photo-Fenton oxidation at neutral pH. Sep Purif Technol, 317, 123877. https://doi.org/10.1016/j.seppur.2023.123877

García-Muñoz, P., López-Maxías, C., Guerra-Rodríguez, S., Carbajo, J., Casas, J. A., and Rodríguez-Chueca, J. (2022). Photocatalytic activation of peroxymonosulfate using ilmenite (FeTiO3) for Enterococcus faecalis inactivation. J Environ Chem Eng, 10(5), 108231. https://doi.org/10.1016/j.jece.2022.108231

Gu, C., Liu, S., Liang, J., Wang, Y., Lu, S., and Ma, J. (2023). Degradation of 1,2,3-trichloropropane by pyrite activating sodium percarbonate and the implications for groundwater remediation. J Environ Chem Eng, 11(1), 109217. https://doi.org/10.1016/j.jece.2022.109217

Guo, H., Stüben, D., and Berner, Z. (2007). Removal of arsenic from aqueous solution by natural siderite and hematite. Appl Geochem, 22(5), 1039–1051. https://doi.org/10.1016/j.apgeochem.2007.01.004

Guo, Q., Zhu, W., Yang, D., Wang, X., Li, Y., Gong, C., Yan, J., Zhai, J., Gao, X., and Luo, Y. (2021). A green solar photo-Fenton process for the degradation of carbamazepine using natural pyrite and organic acid with in-situ generated H2O2. Sci Total Environ, 784, 147187. https://doi.org/10.1016/j.scitotenv.2021.147187

Guo, R., Chen, Y., Liu, B., Han, Y., Gou, J., and Cheng, X. (2022a). Catalytic degradation of lomefloxacin by photo-assisted persulfate activation on natural hematite: Performance and mechanism. Chin Chem Lett, 33(8), 3809–3817. https://doi.org/10.1016/j.cclet.2021.11.061

Guo, R., Xi, B., Guo, C., Liu, W., Lv, N., and Xu, J. (2022b). Comprehensive insight into heterogeneous persulfate activation for environmental pollutants degradation: Approaches and mechanism. Environmental Functional Materials, 1(3), 239–252. https://doi.org/10.1016/j.efmat.2022.12.001

Hajiahmadi, M., Zarei, M., and Khataee, A. (2022). An effective natural mineral-catalyzed heterogeneous electro-Fenton method for degradation of an antineoplastic drug: Modeling by a neural network. Chemosphere, 291, 132810. https://doi.org/10.1016/j.chemosphere.2021.132810

Han, Y., Sun, S., Zhang, B., Du, J., and Duan, X. (2022). Activation of peroxymonosulfate by natural pyrite for efficient degradation of V(IV)-citrate complex in groundwater. J Colloid Interface Sci, 617, 683–693. https://doi.org/10.1016/j.jcis.2022.03.057

Han, H., Li, J., and Santos, H. A. (2023). Recent advances in Fenton and Fenton-like reaction mediated nanoparticle in cancer therapy. Biomedical Technology, 3, 40–51. https://doi.org/10.1016/j.bmt.2022.12.004

He, H., Zhong, Y., Liang, X., Tan, W., Zhu, J., and Wang, C. Y. (2015). Natural Magnetite: an efficient catalyst for the degradation of organic contaminant. Sci Rep, 5, 10139. https://doi.org/10.1038/srep10139

He, P., Zhu, J., Chen, Y., Chen, F., Zhu, J., Liu, M., Zhang, K., and Gan, M. (2021). Pyrite-activated persulfate for simultaneous 2,4-DCP oxidation and Cr(VI) reduction. Chem Eng J, 406, 126758. https://doi.org/10.1016/j.cej.2020.126758

Hou, L., Zhang, H., and Xue, X. (2012). Ultrasound enhanced heterogeneous activation of peroxydisulfate by magnetite catalyst for the degradation of tetracycline in water. Sep Purif Technol, 84, 147–152. https://doi.org/10.1016/j.seppur.2011.06.023

Hou, L., Wang, L., Royer, S., and Zhang, H. (2016). Ultrasound-assisted heterogeneous Fenton-like degradation of tetracycline over a magnetite catalyst. J Hazard Mater, 302, 458–467. https://doi.org/10.1016/j.jhazmat.2015.09.033

Hou, X., Huang, X., Jia, F., Ai, Z., Zhao, J., and Zhang, L. (2017). Hydroxylamine Promoted Goethite Surface Fenton Degradation of Organic Pollutants. Environ Sci Technol, 51(9), 5118–5126. https://doi.org/10.1021/acs.est.6b05906

Hu, L., Wang, P., Zhang, G., Liu, G., Li, Y., Shen, T., and Crittenden, J. C. (2020). Enhanced persulfate oxidation of organic pollutants and removal of total organic carbons using natural magnetite and microwave irradiation. Chem Eng J, 383, 123140. https://doi.org/10.1016/j.cej.2019.123140

Huang, X., Zhu, T., Duan, W., Liang, S., Li, G., and Xiao, W. (2020). Comparative studies on catalytic mechanisms for natural chalcopyrite-induced Fenton oxidation: Effect of chalcopyrite type. J Hazard Mater, 381, 120998. https://doi.org/10.1016/j.jhazmat.2019.120998

Huang, M., Fang, G., Chen, N., and Zhou, D. (2022a). Hydroxylamine promoted hydroxyl radical production and organic contaminants degradation in oxygenation of pyrite. J Hazard Mater, 429, 128380. https://doi.org/10.1016/j.jhazmat.2022.128380

Huang, R., Yang, J., Cao, Y., Dionysiou, D. D., and Wang, C. (2022b). Peroxymonosulfate catalytic degradation of persistent organic pollutants by engineered catalyst of self-doped iron/carbon nanocomposite derived from waste toner powder. Sep Purif Technol, 291, 120963. https://doi.org/10.1016/j.seppur.2022.120963

Jeong, H. Y., Lee, J. H., and Hayes, K. F. (2008). Characterization of synthetic nanocrystalline mackinawite: Crystal structure, particle size, and specific surface area. Geochim Cosmochim Acta, 72(2), 493–505. https://doi.org/10.1016/j.gca.2007.11.008

Jiang, F., Zhang, L., Yue, T., Tang, H., Wang, L., Sun, W., Zhang, C., and Chen, J. (2021). Defect-boosted molybdenite-based co-catalytic Fenton reaction. Inorg Chem Front, 8(14), 3440–3449. https://doi.org/10.1039/D1QI00344E

Jiang, H., Zahmatkesh, S., Yang, J., Wang, H., and Wang, C. (2022a). Ultrasound-enhanced catalytic degradation of simulated dye wastewater using waste printed circuit boards: catalytic performance and artificial neuron network-based simulation. Environ Monit Assess, 195(1), 144. https://doi.org/10.1007/s10661-022-10744-y

Jiang, Y., Ran, J., Mao, K., Yang, X., Zhong, L., Yang, C., Feng, X., and Zhang, H. (2022b). Recent progress in Fenton/Fenton-like reactions for the removal of antibiotics in aqueous environments. Ecotoxicol Environ Saf, 236, 113464. https://doi.org/10.1016/j.ecoenv.2022.113464

Kalantary, R. R., Moradi, M., Pirsaheb, M., Esrafili, A., Jafari, A. J., Gholami, M., Vasseghian, Y., Antolini, E., and Dragoi, E.-N. (2019). Enhanced photocatalytic inactivation of E. coli by natural pyrite in presence of citrate and EDTA as effective chelating agents: Experimental evaluation and kinetic and ANN models. J Environ Chem Eng, 7(1), 102906. https://doi.org/10.1016/j.jece.2019.102906

Kanafin, Y. N., Abdirova, P., Arkhangelsky, E., Dionysiou, D. D., and Poulopoulos, S. G. (2023). UVA and goethite activated persulfate oxidation of landfill leachate. Chem Eng Journal Adv, 14, 100452.

https://doi.org/10.1016/j.ceja.2023.100452

Kang, H., Lee, D., Lee, K.-M., Kim, H.-H., Lee, H., Sik Kim, M., and Lee, C. (2021). Nonradical activation of peroxymonosulfate by hematite for oxidation of organic compounds: A novel mechanism involving high-valent iron species. Chem Eng J, 426, 130743. https://doi.org/10.1016/j.cej.2021.130743

Kang, Z., Jia, X., Zhang, Y., Kang, X., Ge, M., Liu, D., Wang, C., and He, Z. (2022). A Review on Application of Biochar in the Removal of Pharmaceutical Pollutants through Adsorption and Persulfate-Based AOPs. Sustainability, 14(16), Article 16. https://doi.org/10.3390/su141610128

Kermani, M., Mohammadi, F., Kakavandi, B., Esrafili, A., and Rostamifasih, Z. (2018). Simultaneous catalytic degradation of 2,4-D and MCPA herbicides using sulfate radical-based heterogeneous oxidation over persulfate activated by natural hematite (α-Fe 2 O 3 /PS). J Phys Chem Solids, 117, 49–59. https://doi.org/10.1016/j.jpcs.2018.02.009

Khataee, A., Gholami, P., and Sheydaei, M. (2016). Heterogeneous Fenton process by natural pyrite for removal of a textile dye from water: Effect of parameters and intermediate identification. J Taiwan Inst Chem Eng, 58, 366–373. https://doi.org/10.1016/j.jtice.2015.06.015

Khataee, A., Hassandoost, R., and Rahim Pouran, S. (2018). Cerium-substituted magnetite: Fabrication, characterization and sonocatalytic activity assessment. Ultrason Sonochem, 41, 626–640. https://doi.org/10.1016/j.ultsonch.2017.10.028

Lancia, M., Yao, Y., Andrews, C. B., Wang, X., Kuang, X., Ni, J., ... & Zheng, C. (2022). The China groundwater crisis: A mechanistic analysis with implications for global sustainability. Sustainable Horizons, 4, 100042. https://doi.org/10.1016/j.horiz.2022.100042

Labiadh, L., Ammar, S., and Kamali, A. R. (2019). Oxidation/mineralization of AO7 by electro-Fenton process using chalcopyrite as the heterogeneous source of iron and copper catalysts with enhanced degradation activity and reusability. J Electroanal Chem, 853, 113532. https://doi.org/10.1016/j.jelechem.2019.113532

Lai, L., Zhou, H., and Lai, B. (2018). Heterogeneous degradation of bisphenol A by peroxymonosulfate activated with vanadium-titanium magnetite: Performance, transformation pathways and mechanism. Chem Eng J, 349, 633–645. https://doi.org/10.1016/j.cej.2018.05.134

Lai, L., Zhou, H., Zhang, H., Ao, Z., Pan, Z., Chen, Q., Xiong, Z., Yao, G., and Lai, B. (2020). Activation of peroxydisulfate by natural titanomagnetite for atrazine removal via free radicals and high-valent iron-

oxo species. Chem Eng J, 387, 124165. https://doi.org/10.1016/j.cej.2020.124165

Lai, L., He, Y., Zhou, H., Huang, B., Yao, G., and Lai, B. (2021). Critical review of natural iron-based minerals used as heterogeneous catalysts in peroxide activation processes: Characteristics, applications and mechanisms. J Hazard Mater, 416, 125809. https://doi.org/10.1016/j.jhazmat.2021.125809

Li, C., Huang, Y., Dong, X., Sun, Z., Duan, X., Ren, B., Zheng, S., and Dionysiou, D. D. (2019). Highly efficient activation of peroxymonosulfate by natural negatively-charged kaolinite with abundant hydroxyl groups for the degradation of atrazine. Appl Catal B, 247, 10–23. https://doi.org/10.1016/j.apcatb.2019.01.079

Li, W., Yang, S., Wang, W., Liu, Q., He, J., Li, B., Cai, Z., Chen, N., Fang, H., and Sun, S. (2020). Simultaneous removal of Cr(VI) and acid orange 7 from water in pyrite-persulfate system. Environ Res, 189, 109876. https://doi.org/10.1016/j.envres.2020.109876

Li, G., Guo, Y., Jin, Y., Tan, W., Liu, F., and Yin, H. (2021a). Intrinsic mechanisms of calcium sulfite activation by siderite for atrazine degradation. Chem Eng J, 426, 131917. https://doi.org/10.1016/j.cej.2021.131917

Li, T., Abdelhaleem, A., Chu, W., and Xu, W. (2021b). Efficient activation of oxone by pyrite for the degradation of propanil: Kinetics and degradation pathway. J Hazard Mater, 403, 123930. https://doi.org/10.1016/j.jhazmat.2020.123930

Li, Y., Chen, J., Zhong, J., Yang, B., Yang, Z., Shih, K., and Feng, Y. (2022). Acceleration of traces of Fe3+-activated peroxymonosulfate by natural pyrite: A novel cocatalyst for improving Fenton-like processes. Chem Eng J, 435, 134893. https://doi.org/10.1016/j.cej.2022.134893

Lian, W., Yi, X., Huang, K., Tang, T., Wang, R., Tao, X., Zheng, Z., Dang, Z., Yin, H., and Lu, G. (2019). Degradation of tris(2-chloroethyl) phosphate (TCEP) in aqueous solution by using pyrite activating persulfate to produce radicals. Ecotoxicol Environ Saf, 174, 667–674. https://doi.org/10.1016/j.ecoenv.2019.03.027

Liang, X., Zhong, Y., Zhu, S., Zhu, J., Yuan, P., He, H., and Zhang, J. (2010). The decolorization of Acid Orange II in non-homogeneous Fenton reaction catalyzed by natural vanadium–titanium magnetite. J Hazard Mater, 181(1), 112–120. https://doi.org/10.1016/j.jhazmat.2010.04.101

Liang, X., Zhong, Y., Zhu, S., Ma, L., Yuan, P., Zhu, J., He, H., and Jiang, Z. (2012). The contribution of vanadium and titanium on improving methylene blue decolorization through heterogeneous UV-Fenton

reaction catalyzed by their co-doped magnetite. J Hazard Mater, 199–200, 247–254. https://doi.org/10.1016/j.jhazmat.2011.11.007

Liang, Y., Tang, X., Zhu, Q., Han, J., and Wang, C. (2021). A review: Application of tourmaline in environmental fields. Chemosphere, 281, 130780. https://doi.org/10.1016/j.chemosphere.2021.130780

Lin, H., Li, Y., Mao, X., and Zhang, H. (2016). Electro-enhanced goethite activation of peroxydisulfate for the decolorization of Orange II at neutral pH: Efficiency, stability and mechanism. J Taiwan Inst Chem Eng, 65, 390–398. https://doi.org/10.1016/j.jtice.2016.05.050

Liu, H., Chen, T., Zou, X., Qing, C., and Frost, R. L. (2013). Thermal treatment of natural goethite: Thermal transformation and physical properties. Thermochim Acta, 568, 115–121. https://doi.org/10.1016/j.tca.2013.06.027

Liu, H., Li, C., Zhang, T., Xu, Z., Li, Y., Li, B., and Tian, S. (2022a). UV facilitated synergistic effects of polymetals in ore catalyst on peroxymonosulfate activation: Implication for the degradation of bisphenol S. Chem Eng J, 431, 133989. https://doi.org/10.1016/j.cej.2021.133989

Liu, X., Yang, Z., Zhu, W., Yang, Y., and Li, H. (2022b). Catalytic ozonation of chloramphenicol with manganese-copper oxides/maghemite in solution: Empirical kinetics model, degradation pathway, catalytic mechanism, and antibacterial activity. J Environ Manage, 302, 114043. https://doi.org/10.1016/j.jenvman.2021.114043

Liu, X., Liu, S., Qiu, W., Magnuson, J. T., Liu, Z., Yang, G., ... & Zheng, C. (2022c). Cardiotoxicity of PFOA, PFOS, and PFOSA in Early Life Stage Zebrafish: Molecular Changes to Behavioral-level Response. Sustainable Horizons, 3, 100027. https://doi.org/10.1016/j.horiz.2022.100027

Liu, G., Luo, D., Wang, L., Wang, C., Cao, Y., Singh, L., Ahmadzadeh, S., and He, Z. (2023a). Current status and future perspective in electro-Fenton techniques for wastewater treatment: a bibliometric review. Appl Nanosci. https://doi.org/10.1007/s13204-023-02855-w

Liu, Z., An, Y., and Li, X. (2023b). Insight into mechanism of peroxydisulfate activation by natural pyrite: Participation of Fe(IV) and regulation of Fe(III)/Fe(II) cycle by sulfur species. Chemosphere, 314, 137657. https://doi.org/10.1016/j.chemosphere.2022.137657

Loffredo, C. M., Dennehy, M., and Alvarez, M. (2023). Fe-Mn/ZrO2 catalysts: Sulfate-based-advanced oxidation process for the degradation of olive oil industry model pollutants. Catal Commun, 174, 106578. https://doi.org/10.1016/j.catcom.2022.106578

Lu, M.-C. (2000). Oxidation of chlorophenols with hydrogen peroxide in the presence of goethite. Chemosphere, 40(2), 125–130. https://doi.org/10.1016/S0045-6535(99)00213-1

Lu, Y., Ding, C., Guo, J., Gan, W., Chen, P., Chen, R., Ling, Q., Zhang, M., Wang, P., and Sun, Z. (2023). Cobalt-doped ZnAl-LDH nanosheet arrays as recyclable piezo-catalysts for effective activation of peroxymonosulfate to degrade norfloxacin: Non-radical pathways and theoretical calculation studies. Nano Energy, 112, 108515. https://doi.org/10.1016/j.nanoen.2023.108515

Magalhães, F., Pereira, M. C., Botrel, S. E. C., Fabris, J. D., Macedo, W. A., Mendonça, R., Lago, R. M., and Oliveira, L. C. A. (2007). Cr-containing magnetites Fe3−xCrxO4: The role of Cr3+ and Fe2+ on the stability and reactivity towards H2O2 reactions. Appl Catal A Gen, 332(1), 115–123. https://doi.org/10.1016/j.apcata.2007.08.002

Marsac, R., Pasturel, M., and Hanna, K. (2017). Reduction Kinetics of Nitroaromatic Compounds by Titanium-Substituted Magnetite. J Phys Chem C, 121(21), 11399–11406. https://doi.org/10.1021/acs.jpcc.7b01920

Mashayekh-Salehi, A., Akbarmojeni, K., Roudbari, A., Peter van der Hoek, J., Nabizadeh, R., Dehghani, M. H., and Yaghmaeian, K. (2021). Use of mine waste for H2O2-assisted heterogeneous Fenton-like degradation of tetracycline by natural pyrite nanoparticles: Catalyst characterization, degradation mechanism, operational parameters and cytotoxicity assessment. J Clean Prod, 291, 125235. https://doi.org/10.1016/j.jclepro.2020.125235

Mikhlin, Y., Tomashevich, Y., Tauson, V., Vyalikh, D., Molodtsov, S., and Szargan, R. (2005). A comparative X-ray absorption near-edge structure study of bornite, Cu5FeS4, and chalcopyrite, CuFeS2. J Electron Spectros Relat Phenomena, 142(1), 83–88. https://doi.org/10.1016/j.elspec.2004.09.003

Mora, V. C., and Rosso, J. A. (2022). Treatment of PAH-contaminated soil by persulfate: a review. Curr Opin Chem Eng, 37, 100842. https://doi.org/10.1016/j.coche.2022.100842

Munoz, M., Conde, J., de Pedro, Z. M., and Casas, J. A. (2018). Antibiotics abatement in synthetic and real aqueous matrices by H2O2/natural magnetite. Catal Today, 313, 142–147. https://doi.org/10.1016/j.cattod.2017.10.032

Ni, Z., Zhang, C., Ma, H., Liu, J., Wang, Z., Zhu, K., Li, M., and Jia, H. (2022). Facet-dependent photo-degradation of nitro polycyclic aromatic hydrocarbons on hematite under visible light: Participation of environmentally persistent free radicals and reactive oxygen/nitrogen species. Appl Catal B, 318, 121816.

https://doi.org/10.1016/j.apcatb.2022.121816

Niu, B., Wang, N., Chen, Y., Yu, M., Hou, Z., Li, Z., and Zheng, Y. (2021). Tourmaline synergized with persulfate for degradation of sulfadiazine: Influencing parameters and reaction mechanism. Sep Purif Technol, 257, 117893. https://doi.org/10.1016/j.seppur.2020.117893

Novikau, R., and Lujaniene, G. (2022). Adsorption behaviour of pollutants: Heavy metals, radionuclides, organic pollutants, on clays and their minerals (raw, modified and treated): A review. J Environ Manage, 309, 114685. https://doi.org/10.1016/j.jenvman.2022.114685

Pan, Y., Zhang, Y., Hou, M., Xue, J., Qin, R., Zhou, M., and Zhang, Y. (2023). Properties of polyphenols and polyphenol-containing wastewaters and their treatment by Fenton/Fenton-like reactions. Sep Purif Technol, 317, 123905. https://doi.org/10.1016/j.seppur.2023.123905

Peng, J., Yan, J., Chen, Q., Jiang, X., Yao, G., and Lai, B. (2018). Natural mackinawite catalytic ozonation for N, N-dimethylacetamide (DMAC) degradation in aqueous solution: Kinetic, performance, biotoxicity and mechanism. Chemosphere, 210, 831–842. https://doi.org/10.1016/j.chemosphere.2018.07.072

Peng, J., Zhou, H., Liu, W., Ao, Z., Ji, H., Liu, Y., Su, S., Yao, G., and Lai, B. (2020). Insights into heterogeneous catalytic activation of peroxymonosulfate by natural chalcopyrite: pH-dependent radical generation, degradation pathway and mechanism. Chem Eng J, 397, 125387. https://doi.org/10.1016/j.cej.2020.125387

Ponomar, V. P. (2018). Synthesis and magnetic properties of magnetite prepared by chemical reduction from hematite of various particle sizes. J Alloys Compd, 741, 28–34. https://doi.org/10.1016/j.jallcom.2018.01.023

Poza-Nogueiras, V., Rosales, E., Pazos, M., and Sanromán, M. Á. (2018). Current advances and trends in electro-Fenton process using heterogeneous catalysts – A review. Chemosphere, 201, 399–416. https://doi.org/10.1016/j.chemosphere.2018.03.002

Qi, J., Jiang, G., Wan, Y., Liu, J., and Pi, F. (2023). Nanomaterials-modulated Fenton reactions: Strategies, chemodynamic therapy and future trends. Chem Eng J, 466, 142960. https://doi.org/10.1016/j.cej.2023.142960

Rahimi, F., van der Hoek, J. P., Royer, S., Javid, A., Mashayekh-Salehi, A., and Jafari Sani, M. (2021). Pyrite nanoparticles derived from mine waste as efficient catalyst for the activation of persulfates for degradation of tetracycline. J Water Process Eng, 40, 101808.

https://doi.org/10.1016/j.jwpe.2020.101808

Rasoulzadeh, H., Sheikhmohammadi, A., Alinejad, N., and Abtahi, M. (2023). Photo-oxidation degradation of metronidazole in hematite/sulfite system: Mechanism, kinetic, degradation pathway. Optik, 277, 170676. https://doi.org/10.1016/j.ijleo.2023.170676

Saleh, M., Bilici, Z., Kaya, M., Yalvac, M., Arslan, H., Yatmaz, H. C., and Dizge, N. (2021). The use of basalt powder as a natural heterogeneous catalyst in the Fenton and Photo-Fenton oxidation of cationic dyes. Adv Powder Technol, 32(4), 1264–1275. https://doi.org/10.1016/j.apt.2021.02.025

Sang, W., Li, Z., Huang, M., Wu, X., Li, D., Mei, L., and Cui, J. (2020). Enhanced transition metal oxide based peroxymonosulfate activation by hydroxylamine for the degradation of sulfamethoxazole. Chem Eng J, 383, 123057. https://doi.org/10.1016/j.cej.2019.123057

Scheinost, A. C., and Charlet, L. (2008). Selenite reduction by mackinawite, magnetite and siderite: XAS characterization of nanosized redox products. Environ Sci Technol, 42(6), 1984–1989. https://doi.org/10.1021/es071573f

Shi, Y., Hong, S., Li, R., Luo, B., Zhu, H., and Huang, Y. (2023). Insight on the heterogeneously activated H2O2 with goethite under visible light for cefradine degradation: pH dependence and photoassisted effect. Chemosphere, 310, 136799. https://doi.org/10.1016/j.chemosphere.2022.136799

Shokrollahi, H. (2017). A review of the magnetic properties, synthesis methods and applications of maghemite. J Magn Magn Mater, 426, 74–81. https://doi.org/10.1016/j.jmmm.2016.11.033

Silveira, J. E., Garcia-Costa, A. L., Carbajo, J., Ribeiro, A. R., Pliego, G., Paz, W. S., Zazo, J. A., and Casas, J. A. (2022). Nitrate removal in saline water by photo-reduction using natural FeTiO3 as catalyst. Chem Eng Journal Adv, 12, 100387. https://doi.org/10.1016/j.ceja.2022.100387

Song, W., Li, J., Zhang, X., Feng, J., Du, X., Wang, Q., Fu, C., Qiu, W., Wang, Z., and Gao, X. (2022). A feasible approach for azo-dye methyl orange degradation in siderite/H2O2 assisted by persulfate: Optimization using response surface methodology and pathway. J Environ Manage, 308, 114397. https://doi.org/10.1016/j.jenvman.2021.114397

Soufi, A., Hajjaoui, H., Elmoubarki, R., Abdennouri, M., Qourzal, S., and Barka, N. (2022). Heterogeneous Fenton-like degradation of tartrazine using CuFe2O4 nanoparticles synthesized by sol-gel combustion. Appl Surf Sci Adv, 9, 100251. https://doi.org/10.1016/j.apsadv.2022.100251

Sun, F., Liu, H., Wang, H., Shu, D., Chen, T., Zou, X., Huang, F., and Chen, D. (2020a). A novel discovery

of a heterogeneous Fenton-like system based on natural siderite: A wide range of pH values from 3 to 9. Sci Total Environ, 698, 134293. https://doi.org/10.1016/j.scitotenv.2019.134293

Sun, H., Xie, G., He, D., and Zhang, L. (2020b). Ascorbic acid promoted magnetite Fenton degradation of alachlor: Mechanistic insights and kinetic modeling. Appl Catal B, 267, 118383. https://doi.org/10.1016/j.apcatb.2019.118383

Sun, F., Chen, T., Liu, H., Zou, X., Zhai, P., Chu, Z., Shu, D., Wang, H., and Chen, D. (2021a). The pH-dependent degradation of sulfadiazine using natural siderite activating PDS: The role of singlet oxygen. Sci Total Environ, 784, 147117. https://doi.org/10.1016/j.scitotenv.2021.147117

Sun, F., Chen, T., Zou, X., Liu, H., Chu, Z., Shu, D., Wang, H., Huang, F., and Chen, D. (2021b). A quantitative analysis of hydroxyl radical generation as H2O2 encounters siderite: Kinetics and effect of parameters. Appl Geochem, 126, 104893. https://doi.org/10.1016/j.apgeochem.2021.104893

Sun, R., Zhang, X., Wang, C., and Cao, Y. (2021c). Co-carbonization of red mud and waste sawdust for functional application as Fenton catalyst: Evaluation of catalytic activity and mechanism. J Environ Chem Eng, 9(4), 105368. https://doi.org/10.1016/j.jece.2021.105368

Sun, S., Ren, J., Liu, J., Rong, L., Wang, H., Xiao, Y., Sun, F., Mei, R., Chen, C., and Su, X. (2022a). Pyrite-activated persulfate oxidation and biological denitrification for effluent of biological landfill leachate treatment system. J Environ Manage, 304, 114290. https://doi.org/10.1016/j.jenvman.2021.114290

Sun, Y., Zhang, W., Xiang, W., Liu, X., Wu, X., and Zhou, T. (2022b). Catalytic activation of persulfate by mechanically-treated natural pyrite: Revisit on the dominant role of sulfur vacancies and size effect. Chem Eng J, 450, 138269. https://doi.org/10.1016/j.cej.2022.138269

Tian, K., Hu, L., Li, L., Zheng, Q., Xin, Y., and Zhang, G. (2022). Recent advances in persulfate-based advanced oxidation processes for organic wastewater treatment. Chin Chem Lett, 33(10), 4461–4477. https://doi.org/10.1016/j.cclet.2021.12.042

Tuutijärvi, T., Lu, J., Sillanpää, M., and Chen, G. (2009). As(V) adsorption on maghemite nanoparticles. J Hazard Mater, 166(2), 1415–1420. https://doi.org/10.1016/j.jhazmat.2008.12.069

Usman, M., Faure, P., Hanna, K., Abdelmoula, M., and Ruby, C. (2012a). Application of magnetite catalyzed chemical oxidation (Fenton-like and persulfate) for the remediation of oil hydrocarbon contamination. Fuel, 96, 270–276. https://doi.org/10.1016/j.fuel.2012.01.017

Usman, M., Faure, P., Ruby, C., and Hanna, K. (2012b). Remediation of PAH-contaminated soils by magnetite catalyzed Fenton-like oxidation. Appl Catal B, 117–118, 10–17. https://doi.org/10.1016/j.apcatb.2012.01.007

Vafaei Molamahmood, H., Geng, W., Wei, Y., Miao, J., Yu, S., Shahi, A., Chen, C., and Long, M. (2022). Catalyzed H2O2 decomposition over iron oxides and oxyhydroxides: Insights from oxygen production and organic degradation. Chemosphere, 291, 133037. https://doi.org/10.1016/j.chemosphere.2021.133037

Vieira, Y., Silvestri, S., Leichtweis, J., Jahn, S. L., de Moraes Flores, É. M., Dotto, G. L., and Foletto, E. L. (2020). New insights into the mechanism of heterogeneous activation of nano–magnetite by microwave irradiation for use as Fenton catalyst. J Environ Chem Eng, 8(3), 103787. https://doi.org/10.1016/j.jece.2020.103787

Wang, C., Zhang, Y., Yu, L., Zhang, Z., and Sun, H. (2013). Oxidative degradation of azo dyes using tourmaline. J Hazard Mater, 260, 851–859. https://doi.org/10.1016/j.jhazmat.2013.06.054

Wang, Y., Gao, Y., Chen, L., and Zhang, H. (2015). Goethite as an efficient heterogeneous Fenton catalyst for the degradation of methyl orange. Catal Today, 252, 107–112. https://doi.org/10.1016/j.cattod.2015.01.012

Wang, J., and Wang, S. (2018a). Activation of persulfate (PS) and peroxymonosulfate (PMS) and application for the degradation of emerging contaminants. Chem Eng J, 334, 1502–1517. https://doi.org/10.1016/j.cej.2017.11.059

Wang, S., and Wang, J. (2018b). Radiation-induced degradation of sulfamethoxazole in the presence of various inorganic anions. Chem Eng J, 351, 688–696. https://doi.org/10.1016/j.cej.2018.06.137

Wang, P., Liu, X., Qiu, W., Wang, F., Jiang, H., Chen, M., Zhang, W., and Ma, J. (2020). Catalytic degradation of micropollutant by peroxymonosulfate activation through Fe(III)/Fe(II) cycle confined in the nanoscale interlayer of Fe(III)-saturated montmorillonite. Water Res, 182, 116030. https://doi.org/10.1016/j.watres.2020.116030

Wang, C., Huang, R., Sun, R., Yang, J., and Sillanpää, M. (2021a). A review on persulfates activation by functional biochar for organic contaminants removal: Synthesis, characterizations, radical determination, and mechanism. J Environ Chem Eng, 9(5), 106267. https://doi.org/10.1016/j.jece.2021.106267

Wang, C., Sun, R., and Huang, R. (2021b). Highly dispersed iron-doped biochar derived from sawdust

for Fenton-like degradation of toxic dyes. J Clean Prod, 297, 126681. https://doi.org/10.1016/j.jclepro.2021.126681

Wang, C., Sun, R., Huang, R., and Cao, Y. (2021c). A novel strategy for enhancing heterogeneous Fenton degradation of dye wastewater using natural pyrite: Kinetics and mechanism. Chemosphere, 272, 129883. https://doi.org/10.1016/j.chemosphere.2021.129883

Wang, C., Sun, R., Huang, R., and Wang, H. (2021d). Superior fenton-like degradation of tetracycline by iron loaded graphitic carbon derived from microplastics: Synthesis, catalytic performance, and mechanism. Sep Purif Technol, 270, 118773. https://doi.org/10.1016/j.seppur.2021.118773

Wang, C., Yu, G., Chen, H., and Wang, J. (2021e). Degradation of norfloxacin by hydroxylamine enhanced fenton system: Kinetics, mechanism and degradation pathway. Chemosphere, 270, 129408. https://doi.org/10.1016/j.chemosphere.2020.129408

Wang, X., Chen, N., Liu, X., Shi, Y., Ling, C., and Zhang, L. (2021f). Ascorbate guided conversion of hydrogen peroxide to hydroxyl radical on goethite. Appl Catal B, 282, 119558. https://doi.org/10.1016/j.apcatb.2020.119558

Wang, C., Huang, R., Sun, R., Yang, J., and Dionysiou, D. D. (2022a). Microplastics separation and subsequent carbonization: Synthesis, characterization, and catalytic performance of iron/carbon nanocomposite. J Clean Prod, 330, 129901. https://doi.org/10.1016/j.jclepro.2021.129901

Wang, C., Yang, J., Huang, R., and Cao, Y. (2022b). Mechanical activation of natural chalcopyrite for improving heterogeneous Fenton degradation of tetracycline. J Cent South Univ, 29(12), 3884–3895. https://doi.org/10.1007/s11771-022-5199-y

Wang, H., Liao, B., Hu, M., Ai, Y., Wen, L., Yang, S., Ye, Z., Qin, J., and Liu, G. (2022c). Heterogeneous activation of peroxymonosulfate by natural chalcopyrite for efficient remediation of groundwater polluted by aged landfill leachate. Appl Catal B, 300, 120744. https://doi.org/10.1016/j.apcatb.2021.120744

Wang, J., Zhang, Q., Peng, J., Wei, Z., Li, Y., and Wu, X. (2022d). Persulfate activation by copper tailings with hydroxylamine: efficiency, mechanism and DFT calculations. Sep Purif Technol, 297, 121472. https://doi.org/10.1016/j.seppur.2022.121472

Wang, L., Jiang, H., Wang, H., Show, P. L., Ivanets, A., Luo, D., and Wang, C. (2022e). MXenes as heterogeneous Fenton-like catalysts for removal of organic pollutants: A review. J Environ Chem Eng,

10(6), 108954. https://doi.org/10.1016/j.jece.2022.108954

Wang, L., Luo, D., Yang, J., and Wang, C. (2022f). Metal-organic frameworks-derived catalysts for contaminant degradation in persulfate-based advanced oxidation processes. J Clean Prod, 375, 134118. https://doi.org/10.1016/j.jclepro.2022.134118

Wang, W.-M., Li, X., Du, X., and Wu, Q.-Y. (2022g). A feasible approach for azo dye degradation using natural magnetite in heterogeneous Fenton oxidation. Water Cycle, 3, 100–105. https://doi.org/10.1016/j.watcyc.2022.06.002

Wang, X., Bi, X., Yao, N., Elmaci, G., Ertürk, A. S., Lv, Q., ... & Meng, X. (2022h). Doping strategy-tuned non-radical pathway on manganese oxide for catalytic degradation of parabens. Chem Eng J, 442, 136180. https://doi.org/10.1016/j.cej.2022.136180

Wang, H., Fu, S., Choi, C., Zhong, Y., and Schaefer, S. (2023a). Exploring the potential of natural pyrrhotite mineral for electrochemical energy storage. Energy Stor Mater, 54, 421–429. https://doi.org/10.1016/j.ensm.2022.10.058

Wang, L., Luo, D., Hamdaoui, O., Vasseghian, Y., Momotko, M., Boczkaj, G., Kyzas, G. Z., and Wang, C. (2023b). Bibliometric analysis and literature review of ultrasound-assisted degradation of organic pollutants. Sci Total Environ, 876, 162551. https://doi.org/10.1016/j.scitotenv.2023.162551

Wang, L., Lyu, S., and Li, S. (2023c). In-situ observation of structural evolution of single-atom catalysts: From synthesis to catalysis. ChemPhysMater. https://doi.org/10.1016/j.chphma.2023.03.003

Wang, Y., and Dong, X. (2023). PMS activation by natural pyrite for APAP degradation: Underlying mechanism and long-term removal of APAP. Catal Commun, 177, 106661. https://doi.org/10.1016/j.catcom.2023.106661

Wen, X., Liang, Y., Bai, P., Luo, B., Fang, T., Yue, L., An, T., Song, W., and Zheng, S. (2017). First-principles calculations of the structural, elastic and thermodynamic properties of mackinawite (FeS) and pyrite (FeS2). Physica B Condens Matter, 525, 119–126. https://doi.org/10.1016/j.physb.2017.09.007

Wen, J., Duan, F., Yang, L., Liu, X., Huang, Y., Ke, G., He, H., and Yang, H. (2022). The activity and mechanism differences of typical tourmalines in the activation of persulfate for tetracycline degradation. J Solid State Chem, 314, 123383. https://doi.org/10.1016/j.jssc.2022.123383

Wu, J. J., Muruganandham, M., Yang, J. S., and Lin, S. S. (2006). Oxidation of DMSO on goethite catalyst in the presence of H2O2 at neutral pH. Catal Commun, 7(11), 901–906.

https://doi.org/10.1016/j.catcom.2006.03.015

Wu, X., Gu, X., Lu, S., Qiu, Z., Sui, Q., Zang, X., Miao, Z., and Xu, M. (2015). Strong enhancement of trichloroethylene degradation in ferrous ion activated persulfate system by promoting ferric and ferrous ion cycles with hydroxylamine. Sep Purif Technol, 147, 186–193. https://doi.org/10.1016/j.seppur.2015.04.031

Wu, B., Gu, G., Deng, S., Liu, D., and Xiong, X. (2019). Efficient natural pyrrhotite activating persulfate for the degradation of O-isopropyl-N-ethyl thionocarbamate: Iron recycle mechanism and degradation pathway. Chemosphere, 224, 120–127. https://doi.org/10.1016/j.chemosphere.2019.02.062

Wu, B., Deng, S., Wang, H., Gu, G., and Wang, Y. (2020). Insight into the degradation of ammonium dibutyl dithiophosphate by natural pyrrhotite-activated peroxydisulfate: Activation mechanisms, DFT studies. Chem Eng J, 401, 126105. https://doi.org/10.1016/j.cej.2020.126105

Xi, G., Chen, S., Zhang, X., Xing, Y., and He, Z. (2023). Mechanism analysis of efficient degradation of carbamazepine by chalcopyrite-activated persulfate. Environ Sci Pollut Res, 30(5), 13197–13209. https://doi.org/10.1007/s11356-022-23023-7

Xia, D., Li, Y., Huang, G., Yin, R., An, T., Li, G., Zhao, H., Lu, A., and Wong, P. K. (2017a). Activation of persulfates by natural magnetic pyrrhotite for water disinfection: Efficiency, mechanisms, and stability. Water Res, 112, 236–247. https://doi.org/10.1016/j.watres.2017.01.052

Xia, D., Yin, R., Sun, J., An, T., Li, G., Wang, W., Zhao, H., and Wong, P. K. (2017b). Natural magnetic pyrrhotite as a high-Efficient persulfate activator for micropollutants degradation: Radicals identification and toxicity evaluation. J Hazard Mater, 340, 435–444. https://doi.org/10.1016/j.jhazmat.2017.07.029

Xia, D., He, H., Liu, H., Wang, Y., Zhang, Q., Li, Y., Lu, A., He, C., and Wong, P. K. (2018). Persulfate-mediated catalytic and photocatalytic bacterial inactivation by magnetic natural ilmenite. Appl Catal B, 238, 70–81. https://doi.org/10.1016/j.apcatb.2018.07.003

Xu, H., Prasad, M., and Liu, Y. (2009). Schorl: A novel catalyst in mineral-catalyzed Fenton-like system for dyeing wastewater discoloration. J Hazard Mater, 165(1), 1186–1192. https://doi.org/10.1016/j.jhazmat.2008.10.108

Xu, X., Tang, D., Cai, J., Xi, B., Zhang, Y., Pi, L., and Mao, X. (2019). Heterogeneous activation of peroxymonocarbonate by chalcopyrite (CuFeS2) for efficient degradation of 2,4-dichlorophenol in simulated groundwater. Appl Catal B, 251, 273–282. https://doi.org/10.1016/j.apcatb.2019.03.080

Xu, H.-Y., Xu, Y., Zhang, S.-Q., Dai, L.-Y., and Wang, Y. (2023). Fabricating a Fe3O4@HNTs nanoreactor to expedite heterogeneous Fenton-like reactions. Mater Lett, 337, 133985. https://doi.org/10.1016/j.matlet.2023.133985

Yan, N., Liu, F., and Huang, W. (2013). Interaction of oxidants in siderite catalyzed hydrogen peroxide and persulfate system using trichloroethylene as a target contaminant. Chem Eng J, 219, 149–154. https://doi.org/10.1016/j.cej.2012.12.072

Yan, N., Liu, F., Xue, Q., Brusseau, M. L., Liu, Y., and Wang, J. (2015). Degradation of trichloroethene by siderite-catalyzed hydrogen peroxide and persulfate: Investigation of reaction mechanisms and degradation products. Chem Eng J, 274, 61–68. https://doi.org/10.1016/j.cej.2015.03.056

Yan, S., Xiong, W., Xing, S., Shao, Y., Guo, R., and Zhang, H. (2017). Oxidation of organic contaminant in a self-driven electro/natural maghemite/peroxydisulfate system: Efficiency and mechanism. Sci Total Environ, 599–600, 1181–1190. https://doi.org/10.1016/j.scitotenv.2017.05.037

Yang, L., He, L., Xue, J., Ma, Y., Xie, Z., Wu, L., Huang, M., and Zhang, Z. (2020). Persulfate-based degradation of perfluorooctanoic acid (PFOA) and perfluorooctane sulfonate (PFOS) in aqueous solution: Review on influences, mechanisms and prospective. J Hazard Mater, 393, 122405. https://doi.org/10.1016/j.jhazmat.2020.122405

Yang, J., Huang, R., Cao, Y., Wang, H., Ivanets, A., and Wang, C. (2022). Heterogeneous Fenton degradation of persistent organic pollutants using natural chalcopyrite: effect of water matrix and catalytic mechanism. Environ Sci Pollut Res Int, 29(50), 75651–75663. https://doi.org/10.1007/s11356-022-21105-0

Yang, K., Zhai, Z., Liu, H., Zhao, T., Yuan, D., Jiao, T., Zhang, Q., and Tang, S. (2023a). Peracetic acid activation by natural chalcopyrite for metronidazole degradation: Unveiling the effects of Cu-Fe bimetallic sites and sulfur species. Sep Purif Technol, 305, 122500. https://doi.org/10.1016/j.seppur.2022.122500

Yang, R., Zeng, G., Zhou, Z., Xu, Z., and Lyu, S. (2023b). Naphthalene degradation dominated by homogeneous reaction in Fenton-like process catalyzed by pyrite: Mechanism and application. Sep Purif Technol, 310, 123150. https://doi.org/10.1016/j.seppur.2023.123150

Yao, N., Zhao, H., Liu, X., Ertürk, A. S., Elmaci, G., Zhao, P., & Meng, X. (2022). Synergistic adsorption and oxidative degradation of polyvinyl alcohol by acidified OMS-2: Catalytic mechanism, degradation

pathway and toxicity evaluation. Sep Purif Technol, 302, 122047. https://doi.org/10.1016/j.seppur.2022.122047

Yao, J., Liu, J., Wei, Z., Li, Y., Zhou, H., Wang, J., Li, W., Zhang, Q., and Wu, X. (2023). Performance and mechanism of natural chalcopyrite for photocatalytic activation of peroxymonosulfate towards tetracycline degradation. Mater Res Bull, 164, 112275. https://doi.org/10.1016/j.materresbull.2023.112275

Yin, R., Hu, L., Xia, D., Yang, J., He, C., Liao, Y., Zhang, Q., and He, J. (2020). Hydroxylamine promoted Fe(III)/Fe(II) cycle on ilmenite surface to enhance persulfate catalytic activation and aqueous pharmaceutical ibuprofen degradation. Catal Today, 358, 294–302. https://doi.org/10.1016/j.cattod.2019.04.081

Yu, L., Wang, C., Ren, X., and Sun, H. (2014). Catalytic oxidative degradation of bisphenol A using an ultrasonic-assisted tourmaline-based system: Influence factors and mechanism study. Chem Eng J, 252, 346–354. https://doi.org/10.1016/j.cej.2014.05.014

Yu, C., Wen, M., Li, S., Tong, Z., Yin, Y., Liu, X., Li, Y., Wu, Z., and Dionysiou, D. D. (2020). Elbaite catalyze peroxymonosulfate for advanced oxidation of organic pollutants: Hydroxyl groups induced generation of reactive oxygen species. J Hazard Mater, 398, 122932. https://doi.org/10.1016/j.jhazmat.2020.122932

Yuan, G.-E., Qin, Y., Feng, M., Ru, X., and Zhang, X. (2021a). Activation of peroxymonosulfate by natural molybdenite for dye degradation: Identification of reactive species and catalytic mechanism. Environ Technol Innovation, 22, 101403. https://doi.org/10.1016/j.eti.2021.101403

Yuan, G.-E., Qin, Y., Feng, M., Zhang, W., Ru, X., and Zhang, X. (2021b). Synergistic activation of persulfate by natural chalcocite and ferrous ions by promoting the cycling of Fe3+/Fe2+ couple for degradation of organic pollutants. Ecotoxicol Environ Saf, 212, 111975. https://doi.org/10.1016/j.ecoenv.2021.111975

Yuan, T., Wang, X., Zhao, X., Liu, T., Zhang, H., Lv, Y., and Wang, L. (2021c). Efficient degradation of minocycline by natural bornite-activated hydrogen peroxide and persulfate: kinetics and mechanisms. Environ Sci Pollut Res Int, 28(48), 69314–69328. https://doi.org/10.1007/s11356-021-15500-2

Zazo, J. A., García-Muñoz, P., Pliego, G., Silveira, J. E., Jaffe, P., and Casas, J. A. (2020). Selective reduction of nitrate to N2 using ilmenite as a low cost photo-catalyst. Appl Catal B, 273, 118930.

https://doi.org/10.1016/j.apcatb.2020.118930

Zeng, L., Gong, J., Dan, J., Li, S., Zhang, J., Pu, W., and Yang, C. (2019). Novel visible light enhanced Pyrite-Fenton system toward ultrarapid oxidation of p-nitrophenol: Catalytic activity, characterization and mechanism. Chemosphere, 228, 232–240. https://doi.org/10.1016/j.chemosphere.2019.04.103

Zeng, G., Wang, J., Dai, M., Meng, Y., Luo, H., Zhou, Q., Lin, L., Zang, K., Meng, Z., and Pan, X. (2023). Natural iron minerals in an electrocatalytic oxidation system and in situ pollutant removal in groundwater: Applications, mechanisms, and challenges. Sci Total Environ, 871, 161826. https://doi.org/10.1016/j.scitotenv.2023.161826

Zhang, Y., Zhang, K., Dai, C., Zhou, X., and Si, H. (2014). An enhanced Fenton reaction catalyzed by natural heterogeneous pyrite for nitrobenzene degradation in an aqueous solution. Chem Eng J, 244, 438–445. https://doi.org/10.1016/j.cej.2014.01.088

Zhang, L., Verstraete, W., de Lourdes Mendoza, M., Lu, Z., Liu, Y., Huang, G., and Cai, L. (2016). Decrease of dissolved sulfide in sewage by powdered natural magnetite and hematite. Sci Total Environ, 573, 1070–1078. https://doi.org/10.1016/j.scitotenv.2016.08.206

Zhang, Y., Shi, J., Xu, Z., Chen, Y., and Song, D. (2018). Degradation of tetracycline in a schorl/H2O2 system: Proposed mechanism and intermediates. Chemosphere, 202, 661–668. https://doi.org/10.1016/j.chemosphere.2018.03.116

Zhang, Y., Chen, T., Zhao, Y., Chen, D., Zhou, Y., and Liu, H. (2019). Catalytic effect of siderite on H2O2 oxidation of carmine dye: Performance, mechanism and kinetics. Appl Geochem, 106, 26–33. https://doi.org/10.1016/j.apgeochem.2019.04.022

Zhang, W., Tang, G., Yan, J., Zhao, L., Zhou, X., Wang, H., Feng, Y., Guo, Y., Wu, J., Chen, W., Yuan, N., and Li, M. (2020a). The decolorization of methyl orange by persulfate activated with natural vanadium-titanium magnetite. Appl Surf Sci, 509, 144886. https://doi.org/10.1016/j.apsusc.2019.144886

Zhang, X., Deng, H., Zhang, G., Yang, F., and Yuan, G.-E. (2020b). Natural bornite as an efficient and cost-effective persulfate activator for degradation of tetracycline: Performance and mechanism. Chem Eng J, 381, 122717. https://doi.org/10.1016/j.cej.2019.122717

Zhang, J., Zhao, W., Li, Z., Lu, G., and Zhu, M. (2021a). Visible-light-assisted peroxymonosulfate activation over Fe(II)/V(IV) self-doped FeVO4 nanobelts with enhanced sulfamethoxazole degradation: Performance and mechanism. Chem Eng J, 403, 126384. https://doi.org/10.1016/j.cej.2020.126384

Zhang, Y., Zhao, H., Wen, J., Ding, S., and Wang, W. (2021b). Insights into the nonradical degradation mechanisms of antibiotics in persulfate activation by tourmaline. Sep Purif Technol, 270, 118772. https://doi.org/10.1016/j.seppur.2021.118772

Zhang, H., Wang, X., Zhao, X., Dong, Y., Wang, W., and Wang, L. (2022a). Dolomite as a low-cost peroxymonosulfate activator for the efficient degradation of tetracycline: Performance, mechanism and toxicity evolution. J Water Process Eng, 49, 103110. https://doi.org/10.1016/j.jwpe.2022.103110

Zhang, J.-M., Liu, T.-L., Huang, Y.-H., and Wei, X.-M. (2022b). A comparison study of the structural, electronic and mechanical properties of the pure pyrite FeS2 and oxygen doped pyrite FeO0.25S1.75 under pressure range from 0 to 25 GPa. Physica B Condens Matter, 633, 413710. https://doi.org/10.1016/j.physb.2022.413710

Zhang, Q., Zheng, D., Bai, B., Hu, N., and Wang, H. (2022c). Solar-driven photothermal-Fenton removal of ofloxacin through waste natural pyrite with dual-function. Colloids Surf A Physicochem Eng Asp, 641, 128574. https://doi.org/10.1016/j.colsurfa.2022.128574

Zhang, L., Bi, X., Wang, Z., Ertürk, A. S., Elmaci, G., Zhao, H., ... & Meng, X. (2022d). Brønsted-acid sites promoted degradation of phthalate esters over MnO2: Mineralization enhancement and aquatic toxicity assessment. Chemosphere, 291, 132740. https://doi.org/10.1016/j.chemosphere.2021.132740

Zheng, R., Li, J., Zhu, R., Wang, R., Feng, X., Chen, Z., Wei, W., Yang, D., and Chen, H. (2022a). Enhanced Cr(VI) reduction on natural chalcopyrite mineral modulated by degradation intermediates of RhB. J Hazard Mater, 423, 127206. https://doi.org/10.1016/j.jhazmat.2021.127206

Zheng, X., Niu, X., Zhang, D., Ye, X., Ma, J., Lv, M., and Lin, Z. (2022b). Removal of Microcystis aeruginosa by natural pyrite-activated persulfate: Performance and the significance of iron species. Chem Eng J, 428, 132565. https://doi.org/10.1016/j.cej.2021.132565

Zhong, D., Feng, W., Ma, W., Liu, X., Ma, J., Zhou, Z., Du, X., and He, F. (2022). Goethite and lepidocrocite catalyzing different double-oxidant systems to degrade chlorophenol. Environ Sci Pollut Res Int, 29(48), 72764–72776. https://doi.org/10.1007/s11356-022-20855-1

Zhong, C., Jiang, Y., Liu, Q., Sun, X., and Yu, J. (2023). Natural siderite derivatives activated peroxydisulfate toward oxidation of organic contaminant: A green soil remediation strategy. J Environ Sci, 127, 615–627. https://doi.org/10.1016/j.jes.2022.06.030

Zhou, W., Li, Y., Zhang, M., Ying, G.-G., and Feng, Y. (2022). Highly Efficient Degradation of

Sulfisoxazole by Natural Chalcopyrite-Activated Peroxymonosulfate: Reactive Species and Effects of Water Matrices. Water, 14(21), Article 21. https://doi.org/10.3390/w14213450



https://dspace.org/

Harnessing the power of natural minerals: A comprehensive review of their application as heterogeneous catalysts in advanced oxidation processes for organic pollutant degradation

Liu, Hongwen; Li, Xingyang; Zhang, Xiuxiu; Coulon, Frederic; Wang, Chongqing

2023-10-01
Elsevier
https://doi.org/10.1016/j.chemosphere.2023.139404
Liu H, Li X, Zhang X, et al., (2023) Harnessing the power of natural minerals: A comprehensive review of their application as heterogeneous catalysts in advanced oxidation processes for organic pollutant degradation. Chemosphere, Volume 337, October 2023, Article number 139404

Downloaded from a DSpace repository. https://dspace.org/